FINAL Report D

TRyy1317

Project Title: Recycled Concrete Aggregate (RCA) for Infrastructure Elements

Report D: Shear Behavior of RCA Concrete

Prepared for
Missouri Department of Transportation
Construction and Materials

Missouri University of Science and Technology, Rolla, Missouri

May 2014

ABSTRACT

Sustainability is at the forefront of our society. Unfortunately, concrete, our most common construction material uses a significant amount of non-renewable resources. Consequently, many researchers have investigated the use of recycled materials in the production of concrete such as recycled aggregate.

Most research to date has consisted only of the evaluation of the strength and durability of recycled aggregate concrete (RAC) mixtures, while only a limited number of studies have implemented full-scale testing of specimens constructed with RAC to determine its potential use in the industry. For this research, a laboratory testing program was developed to investigate the shear performance of reinforced concrete (RC) beams constructed with RAC. The experimental program consisted of 18 tests performed on full-scale RC beams. The principal parameters investigated were: (1) concrete type (RAC or conventional concrete (CC)) and (2) amount of longitudinal (flexural) reinforcement. The full-scale test results were compared to the theoretical results using design approaches contained in several codes common to North America as well as a shear database of CC specimens.

Analysis of the test data indicates that replacing more than 50% of coarse natural aggregates with RCA results in diminished shear strength. This result suggests that the existing equations for shear capacity as reported in AASHTO LRFD and ACI 318 may require additional modification factors to account for diminished shear strength when aggregate replacement levels exceed 50%. This diminished shear strength is likely the result of a double interfacial transition zone when using recycled concrete as aggregate.

TABLE OF CONTENTS

Page

LIST OF ILLUSTRATIONS

Figure Page

LIST OF TABLES

Table Page

NOMENCLATURE

Symbol	Description
A	Angular coefficient of linear regression plot (Equation 3-34)
A_c	Area of concrete on flexural tension side
A_p	Area of prestressing steel
A_{ps}	Area of prestressing steel
A_s	Area of longitudinal reinforcement
A'_s	Area of compression reinforcement
A_{sl}	Area of longitudinal reinforcement
A_{sw}	Steel vertical reinforcement area
A_v	Steel vertical reinforcement area
A_{vi}	Cross-sectional area in the i^{th} stirrup crossing the critical crack
$A_{v,min}$	Minimum shear reinforcement area
a	Aggregate size (Equation 3-18)
a	Depth of equivalent rectangular stress block
a	Shear span
$\underline{a}$	Critical crack length
a/d	Shear span-to-depth ratio
a_0	Notch depth
a_0/d	Notch depth-to-depth ratio
a_c	Critical position of diagonal crack
a_g	Aggregate size (AASHTO LRFD, 2010)

a_s	Shear span
B	Coefficient obtained through linear regression plot (Equation 3-27)
B	Width of cross-section
b	Width of cross-section
b_v	Effective width of cross-section
b_w	Width of cross-section
C_i	Measured initial compliance
C_u	Unloading compliance
c	Distance from extreme compression fiber to the neutral axis
c_v	Concrete cover for transverse reinforcement
c_x	Concrete cover for longitudinal reinforcement
D	Diameter of the cylinder
D_{max}	Aggregate size
d	Characteristic dimension of structure (Equation 3-28)
d	Effective depth of cross-section
d'	Distance from extreme compression fiber to centroid of longitudinal compression reinforcement
d_0	Coefficient determined experimentally (Bazant and Pfeiffer, 1987)
d_{agg}	Aggregate size
d_{bv}	Diameter of transverse steel reinforcement
d_{bx}	Diameter of longitudinal steel reinforcement
d_v	Effective shear depth (AASHTO LRFD, 2010)
E	Modulus of elasticity of the concrete (Equation 3-34)

E_c	Modulus of elasticity of the concrete
E_p	Modulus of elasticity of the prestressing steel
E_s	Modulus of elasticity of the steel
F_c	Concrete compressive force
F_s	Longitudinal reinforcement force
f_1	Principal tensile stress of the concrete
f_2	Principal compressive stress of the concrete
$f_{2,max}$	Maximum principal compressive stress of the concrete
f'_c	Compressive strength of the concrete
f_{ci}	Compressive stress on crack surface
f_{cr}	Concrete stress at cracking
f_{ct}	Tensile strength of the concrete
f_{cx}	Horizontal concrete stress
f_{cy}	Vertical concrete stress
f_{p0}	Parameter to account for level of prestressing (AASHTO LRFD, 2010)
f_t	Splitting tensile strength of the concrete
f'_t	Tensile strength of the concrete
f_v	Tensile stress in the stirrups
f_{vi}	Stress in the i^{th} stirrup crossing the critical crack
f_y	Yield stress of steel
f_{yt}	Yield stress of transverse steel reinforcement
G	Fracture energy consumption (Equation 3-36)
G_F	Fracture energy (Work-of-fracture method)

G_f	Fracture energy (Size effect method)
G_f	Fracture energy (Two parameter method)
G_s	Shear modulus of steel
$g_f(\alpha_0)$	Non-dimensional energy release rate (Equation 3-34)
H	Height of cross-section
H_0	Thickness of clip gauge holder
h	Height of cross-section
jd	Distance between resultants of internal compressive and tensile forces on a cross-section
K_{Ic}	Stress intensity factor
k	Parameter to reflect size effect (Equation 3-27)
k_1	Coefficient that characterizes bond properties of bars (Equations 3-20)
k_3	Empirical coefficient (Equation 3-49)
L	Length of the beam
M_{exp}	Experimentally determined total moment applied to specimen
M_f	Factored shear moment
M_n	Nominal moment capacity
M_u	Factored shear moment
MOR	Modulus of rupture of the concrete
N_h	Tensile force in longitudinal reinforcement
N_u	Factored axial force
n	Curve-fitting factor (Collins and Mitchell, 1997)
n	Number of data points

P	Maximum load at failure
P_{max}	Measured peak load
S	Specimen loading span
s	Center-to-center spacing of steel stirrups
s	Shear crack sliding
s	Standard deviation
s_{mv}	Average spacing of cracks perpendicular to transverse reinforcement
s_{mx}	Average spacing of cracks perpendicular to longitudinal reinforcement
s_x	Crack spacing parameter (AASHTO LRFD, 2010)
s_x	Spacing of longitudinal steel reinforcement
s_{xe}	Effective crack spacing
s_z	Crack spacing parameter (CSA A23.3, 2004)
s_{ze}	Effective crack spacing
s_θ	Crack spacing
$T_{n,1}$	Test criterion (ASTM E178 [2008])
V	External shear force
V_c	Concrete contribution to shear strength
V_{cr}	Ultimate shear force
V_{cz}	Uncracked concrete force
V_d	Longitudinal reinforcement dowel force
V_f	Factored shear force
V_i	Interlock forces
V_n	Nominal shear strength

$V_{n,exp}$	Experimentally determined total shear resistance
$V_{n,max}$	Maximum nominal shear strength
V_p	Vertical component of prestressing force
V_r	Nominal shear resistance
V_s	Steel contribution to shear strength
V_{test}	Experimentally determined total shear resistance
V_u	Factored shear force
v	Shear stress
v_{ci}	Shear transferred by aggregate interlock
$v_{ci,max}$	Maximum shear transferred by aggregate interlock
v_{cxy}	Shear stress on concrete layer face
W	Total energy dissipated (Equation 3-26)
W_{ext}	Work of external force (Equation 3-36)
w	Average crack width (Equation 3-18)
w	Crack opening (Einsfeld and Velasco, 2006)
w	Width of idealized prismatic strut
w/c	Water-to-cement ratio
w/cm	Water-to-cementitious material ratio
$\overline{x}$	Arithmetic average
y	Diagonal crack extent (Equation 3-38)
z	Inner level arm
α_0	Aggregate shape factor (Equation 3-51)
α_0	Relative notch length (Equation 3-35)

α_1	Coefficient for bond characteristics of reinforcement (Vecchio and Collins, 1993)
α_2	Coefficient for type of loading (Vecchio and Collins, 1993)
β	Brittleness number (Equation 3-27)
β	Concrete softening coefficient (Equation 3-14)
β	Shear retention factor (AASHTO LRFD, 2010)
γ_{xy}	Shear strain
δ_e	Variation of unbounded length
δ_s	Unbonded length of reinforcement
ε_0	Concrete strain at peak stress
ε_1	Principal tensile strain in concrete
$\bar{\varepsilon_1}$	Uniaxial tensile strain in the perpendicular direction
ε_2	Principal compressive strain in concrete
ε_c	Compressive strain in the concrete
ε'_c	Compressive strain in the concrete
ε_{cr}	Crack strain in concrete
ε_s	Measured longitudinal strain at the center of gravity at the bottom steel reinforcement
ε_s	Strain in the tension reinforcement
ε'_s	Measured longitudinal strain at the top steel reinforcement
ε'_s	Strain in the compression reinforcement
ε_{sm}	Measured longitudinal strain at the bottom steel reinforcement
ε_{td}	Transverse strain

ε_x	Longitudinal strain (AASHTO LRFD, 2010)
ε_x	Strain in the x-direction
ε_{xx}	Horizontal strain
ε_{xy}	Shear strain
ε_y	Strain in the y-direction
ε_{yield}	Yield strain of steel
ε_{yy}	Vertical strain
θ	Shear crack angle
θ_c	Shear crack angle
ξ	Concrete softening coefficient
$\xi f'_c$	Concrete peak softened stress
$\xi \varepsilon_0$	Concrete softened compressive strain
ρ_L	Longitudinal reinforcement ratio
ρ_s	Longitudinal reinforcement ratio
ρ_v	Transverse reinforcement ratio
ρ_w	Longitudinal reinforcement ratio
ρ_x	Longitudinal reinforcement ratio
σ_N	Nominal stress at failure (Equation 3-27)
Σ_s	Reduced cross section of rebar (Equation 3-38)
$\emptyset$	Capacity reduction factor
$\emptyset_c$	Capacity reduction factor
$\emptyset_s$	Capacity reduction factor
Γ	Fracture energy per unit length of splitting crack extension

1. INTRODUCTION

1.1. BACKGROUND

The construction of buildings, bridges, and roadways continues to increase in the twenty-first century, especially in areas with ever-growing populations. Existing structures and highways require repair or replacement as they reach the end of their service life or simply no longer satisfy their intended purpose due to the growing population. As modern construction continues, two pressing issues will become more apparent to societies: an increasing demand for construction materials, especially concrete and asphalt aggregates, and an increasing production of construction and demolition waste. Already, the Federal Highway Administration (FHWA 2004) estimates that two billion tons of new aggregate are produced each year in the United States. This demand is anticipated to increase to two and a half billion tons each year by 2020. With such a high demand for new aggregates, the concern arises of the depletion of the current sources of natural aggregates and the availability of new sources. Similarly, the construction waste produced in the United States is expected to increase. From building demolition alone, the annual production of construction waste is estimated to be 123 million tons (FHWA 2004). Currently, this waste is most commonly disposed of in landfills.

To address both the concern of increasing demand for new aggregates and increasing production of waste, many states have begun to recognize that a more sustainable solution exists in recycling waste concrete for use as aggregate in new concrete, or recycled concrete aggregates (RCA). The solution helps address the question

of how to sustain modern construction demands for aggregates as well as helps to reduce the amount of waste that enters already over-burdened landfills.

Based on a survey by FHWA in 2002, many states had begun to implement recycled concrete aggregates in some ways in new construction. As shown in **Figure 1.1**, most states had recognized the many uses of RCA as a raw material, such as for rip-rap, soil stabilization, pipe bedding, and even landscape materials. As shown in **Figure 1.2**, many states had gone a step further in integrating RCA into roadway systems for use as aggregate base course material. However, as shown in **Figure 1.3**, only a small number of states had begun using RCA in Portland cement concrete for pavement construction. However, over the intervening 12 years, the use of RCA has increased significantly, particularly within the last 5 years, and the Missouri Department of Transportation (MoDOT) has instituted a very aggressive program to increase the use of recycled materials in transportation-related construction. However, there are currently no acceptable standards or guidelines in the U.S. for utilizing RCA in structural concrete.

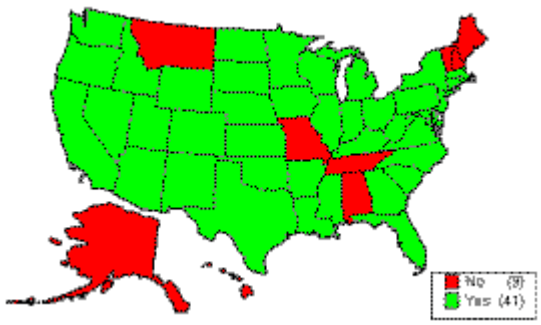

Figure 1.1: States using RCA as Aggregate

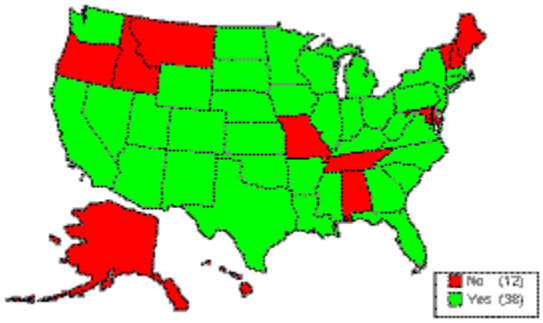

Figure 1.2: States using RCA as Base Aggregate

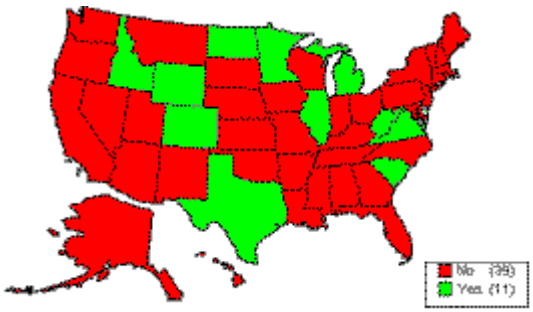

Figure 1.3: States using RCA in PC Concrete

1.2. CONCERNS WITH RECYCLED AGGREGATE CONCRETE

RCAs are composed of both the original, or virgin, aggregate, as well as mortar which remains adhered to the surface of the aggregate. In the production of RCA, the removal of all this residual mortar would prove costly and detrimental to the integrity of the virgin aggregates within the concrete. Therefore, residual mortar is inevitable. Research has shown that this residual mortar causes high water absorption, low density, low specific gravity, and high porosity in RCAs compared to natural aggregates. These effects in the recycled aggregate can decrease hardened concrete properties of recycled aggregate concrete (RAC). According to Abbas et al. (2008), the amount of residual

mortar on the RCA can significantly affect the mechanical and durability properties of RAC. To reduce the negative impacts of this residual mortar, new mix design methods such as the equivalent mortar volume method can be used.

Due to the variety of sources of RCA and the various functions, environment, and wear of the concrete structures and pavements from which the RCA can be obtained, characterizing this aggregate can be very difficult. Controlled studies must be performed to account for each of these variables on a regional basis, such as for each state's Department of Transportation, so that the aggregates within the area can be adequately characterized.

1.3. OBJECTIVE AND SCOPE OF WORK

The main ***objective*** of this research study was to evaluate the shear behavior and response of RCA through material, component, and full-scale testing. This objective included a study and evaluation of current analytical models used to predict the shear response of conventional Portland-cement concrete as applied to RCA, including recommended modifications.

The following ***scope of work*** was implemented in order to achieve the objective of the research study:

- Perform a literature review;
- Develop a research plan;
- Develop mix designs for both conventional and RAC;
- Evaluate the fresh and hardened properties of several RAC and CC mixes;
- Design and construct small and full-scale specimens;

- Test specimens to failure;
- Record and analyze data from tests;
- Compare test results to current guidelines and previous research findings;
- Provide greater insight into the shear resistance mechanisms and quantify their effect;
- Evaluate the applicability of current analytical models to predict the shear behavior and response of RAC;
- Develop conclusions and recommendations; and
- Prepare this report to document the details, results, findings, conclusions, and recommendations of this study.

1.4. RESEARCH METHODOLOGY

The proposed research methodology included six (6) tasks necessary to successfully complete the study. They are as follows:

Task #1: Perform a literature review. The goal of the literature review was to become familiarized with testing methods and results from previous studies. This knowledge was used for a better understanding of the behavior of the specimens, to avoid mistakes, as well as to provide support for comparisons.

Task #2: Develop RAC and CC mix designs. The purpose of this task was to develop RAC mix designs that maximized the percentage of recycled concrete aggregate, but that still fulfilled typical construction needs, such as early strength development. Conventional concrete mix designs served as controls during this study. ACI 211.1-91 formed the basis for developing the mix designs.

Task #3: Perform material and component testing. A number of hardened concrete property tests were completed to evaluate the performance of the RAC mix and determine the validity of using these tests to predict the performance of concretes containing recycled concrete aggregate.

Task #4: Perform full-scale testing. This task was critical as current shear design provisions for reinforced concrete are largely empirical. This task involved the construction and testing of full-scale specimens to confirm the potential of RAC. The full-scale specimens included beam specimens for shear testing only. These specimens were constructed with materials from the local Ready Mix Concrete plant to validate the ability of transferring the mix designs from the laboratory to the field. In order to compare the shear strength of conventional and RAC, full-scale beams were tested in a third point loading configuration. These beams were designed to fail in shear by increasing the flexural reinforcement. Different longitudinal reinforcement ratios were also considered. Strain gauges were applied to the flexural reinforcement, and the maximum load applied to the beam was also recorded and used to calculate the strength of the beams and the different shear components.

Task #5: Analyze test data. The material, component, and full-scale test results were analyzed to evaluate the shear behavior and response of RAC compared to conventional Portland-cement concrete. The test data included: concrete compressive and tensile strength, modulus of rupture (MOR), shear force-deflection plots, crack formation and propagation, and reinforcement strains.

Task #6: Develop findings, conclusions, and recommendations. This task synthesized the results of the previous tasks into findings, conclusions, and recommendations on the shear behavior and response of RAC.

1.5. REPORT OUTLINE

This report includes six chapters. This section will discuss the information that will be presented in more detail throughout this document.

Chapter 1 acts as an introduction to the report. This introduction contains a brief background of recycled aggregate. It also discusses the research objective, scope of work, and research plan.

Chapter 2 includes information from previous research performed on the characterization of recycled aggregate and its applications as a coarse aggregate in concrete.

Chapter 3 presents information from previous research performed on shear design including the different methods and approaches formulated to address this phenomenon. Four different approaches are presented: truss model, Strut and Tie Model (STM), Modified Compression Field Theory (MCFT), and fracture mechanics approach. A collection of three design code philosophies that can be found in North America are also presented in this chapter.

Chapter 4 includes information about the experimental program. The experimental program consisted of 12 tests performed on full-scale reinforced concrete beams as well as material and component testing to determine hardened concrete properties such as compressive strength, splitting tensile strength, and flexural strength.

This chapter also describes the fabrication process, test set-up, and instrumentation for the full-scale testing.

Chapter 5 presents the test results and the different analyses used to investigate the shear resistance mechanisms. The overall behavior of the specimens is described first, with a focus on crack patterns, failure modes, and shear strength.

Chapter 6 concludes this document, summarizing the findings and conclusions of this study and proposing recommendations and future research.

2. LITERATURE REVIEW ON RECYCLED AGGREGATE

2.1. GENERAL

Conventional Portland-cement concrete is produced more than any other material in the world. It is used in every civil engineering field for applications such as pavements, dams, bridges, and buildings because of its versatility, strength, and durability. In this chapter, a brief review is presented of the research performed on concrete mixtures containing recycled aggregate as coarse aggregate.

Concrete with recycled aggregate can be produced to achieve desired strengths at various ages, with a given water-cementitious ratio, aggregate size, air content, and slump as it is done for conventional concrete.

2.2. USE OF RECYCLED AGGREGATE AS COARSE AGGREGATE

Recently, there has been an increasing trend toward the use of sustainable materials. Sustainability helps the environment by reducing the consumption of non-renewable natural resources. Concrete – the second most consumed material in the world after water – uses a significant amount of non-renewable resources. As a result, numerous researchers have investigated the use of recycled materials in the production of concrete such as fly ash and recycled aggregate.

Unfortunately, global data on concrete waste generation is not available, but construction and demolition waste accounts for around 900 million tonnes every year just in Europe, the US, and Japan (WBCSD 2012). Recycling concrete not only reduces using virgin aggregate but also decreases the amount of waste in landfills.

In general, RCA has lower specific gravity and unit weight and considerably higher absorption and porosity compared to natural aggregates. These factors need to be taken into account when designing concrete mixes containing RCA.

2.3. PREVIOUS STUDIES RELATED TO RAC

Comprehensive research has been done on both the fresh and hardened properties of recycled aggregate concrete (RAC), but limited, and often contradictory, research has been performed on the structural behavior of RAC. The early research on structural performance of RAC was published in Japan (Kikuchi et al.1988). Maruyama et al. (2004) tested beams with different longitudinal reinforcement ratios ranging between 2.4% and 4.2%. They also investigated three different water/cementitious material ratios, w/cm, (0.30, 0.45, and 0.60) for their mix designs. They reported that the crack patterns and failure modes of the RAC beams were identical with the conventional concrete (CC) beams. The RAC beams without stirrups showed 10-20% lower shear strength compared with the CC beams.

Gonzalez-Fonteboa et al. (2007) tested eight beams with 3% longitudinal reinforcement ratio and 50% recycled coarse aggregate. Results of their study showed that in terms of both deflection and ultimate shear strength, no significant difference was observed between the RAC and CC beams, but they observed notable splitting cracks along the tension reinforcement. They concluded that existing code provisions for shear can be used for the RAC beams. Gonzalez-Fonteboa et al. (2009) repeated the previous study except for adding 8% silica fume to the mix designs. They observed that notable

splitting cracks along the tension reinforcements were mitigated by the addition of silica fume.

Fathifazl et al. (2009) used the equivalent mortar volume (EMV) method for their mix designs. They used both limestone (63.5% recycled aggregate replacement) and river gravel (74.3% recycled aggregate replacement) as a coarse aggregate for their mix designs. They tested beams with four different shear span-to-depth ratios ranging between 1.5 and 4, and also with four different effective depths (250, 375, 450, and 550 mm) to investigate size effect. They reported superior shear strength for the RAC beams. They also concluded that current code provisions for shear conservatively predicted the capacities of the RAC beams.

Choi et al. (2010) evaluated the shear strength of 20 reinforced concrete beams with different span-to-depth ratios (1.50, 2.50, and 3.25), longitudinal reinforcement ratios (0.53%, 0.83%, and 1.61%), and RCA replacement ratios (0%, 30%, 50%, and 100%). Results of their study showed that the shear strength of the RAC beams was lower than that of the CC beams with the same reinforcement ratio and shear span-to-depth ratio. They reported that beams with smaller span-to-depth ratios and higher percentage of recycled aggregate showed a higher reduction in shear strength.

Schubert et al. (2012) studied 14 slabs (0.2 x 0.5 x 2.3 m) with 100% recycled coarse aggregate under four point load condition. They concluded that RAC slabs can be designed using the same design equations as for CC.

Xiao et al. (2012) tested 32 shear push-off specimens with different percentages of recycled coarse aggregate replacement. They reported no significant difference observed in terms of shear stress-slip curves, crack propagation path, and shear transfer

performance across cracks between the RAC and CC specimens. They also concluded that recycled aggregate replacement up to 30% did not affect ultimate shear load, but for higher percentages of RCA replacement, the ultimate shear load decreased.

2.4. CONCLUDING REMARKS

The literature review reported different results (in some cases contradictory) in terms of shear strength when recycled aggregate was used in concrete. Some research showed using recycled aggregate instead of virgin aggregate in concrete had no effect on shear strength of RAC. Other researchers reported RAC showed lower shear strength and only Fathifazl et al. (2009) used the EMV method and reported superior shear strength for RAC compared with CC.

3. LITERATURE REVIEW ON SHEAR

3.1. GENERAL

The main subject of this document is the shear behavior of reinforced concrete (RC) beams composed of RAC. The current shear design methods and guidelines are presented in this chapter. Four different approaches are presented: truss model, Strut and Tie Model (STM), Modified Compression Field Theory (MCFT), and fracture mechanics approach. A collection of three design code philosophies that can be found in North America will also be used in the evaluation of the shear strength. Some of these guidelines rely on empirical formulas, such as the ACI 318-11, while others, such as the AASHTO LRFD-10 and CSA A23.3-04, rely more on concrete models such as the MCFT.

3.2. FACTORS AFFECTING SHEAR BEHAVIOR

Shear strength is controlled by the presence of web reinforcement, longitudinal reinforcement, coarse aggregate size, presence of axial loads, depth of the member, tensile strength of the concrete, and shear span to depth ratio (a/d). Some of these parameters are included in design equations and others are not.

Web reinforcement, typically called stirrups, is used to increase the shear strength of concrete beams and to ensure flexural failure. This is necessary due to the explosive and sudden nature of shear failures, compared with flexural failures which tend to be more ductile. Web reinforcement is normally provided as vertical stirrups and is spaced at varying intervals along a beam depending on the shear requirements. Alternatively, this reinforcement may be provided as inclined longitudinal bars. In general, small sized bars

such as #3 and #4 are used in a U-shaped configuration that may be open or closed, or used as multiple legs.

Shear reinforcement has very little effect prior to the formation of diagonal cracks. However after cracking, the web reinforcement enhances the beam in the following ways (Nilson et al., 2004):

- The stirrups crossing the crack help in resisting the shear force.
- The stirrups restrict the growth of the cracks and reduce their penetration further into the compression zone.
- The stirrups oppose widening of the cracks, which helps to maintain aggregate interlock within the concrete.
- The presence of stirrups provides extra restraint against the splitting of concrete along the longitudinal bars due to their confinement effect.

The longitudinal reinforcement ratio (ρ_L) affects the extent and the width of the flexural cracks. If this ratio is small, the flexural cracks extend higher into the beam and open wider. When the crack width increases, the components of shear decrease, because they are transferred either by dowel action or by shear stresses on the crack surfaces.

The coarse aggregate type and size noticeably affect the shear capacity, especially for beams without stirrups. Lightweight aggregate has a lower tensile strength than normal aggregate. The shear capacity of a concrete beam with no stirrups is directly related to the tensile strength, therefore, the failure due to mortar cracking, which is more desirable, could be preceded by aggregate failure instead. The aggregate size also affects the amount of shear stresses transferred across the cracks. Large diameter aggregate

increases the roughness of the crack surfaces, allowing higher shear stresses to be transferred (Wight and MacGregor, 2009).

Researchers have concluded that axial compression serves to increase the shear capacity of a beam while axial tension greatly decreases the strength. As the axial compressive force is increased, the onset of flexural cracking is delayed, and the flexural cracks do not penetrate as far as into the beam (Wight and MacGregor, 2009).

The size of the beam affects the shear capacity at failure. If the overall depth of a beam is increased, it could result in a smaller shear force at failure. The reasoning is that when the overall depth of a beam increases, so do the crack width and crack spacing, causing loss of aggregate interlock. This condition is known as a size effect.

The tensile strength of the concrete (f_{ct}) also affects the shear strength. Because of the low tensile strength of the concrete, diagonal cracking develops along planes perpendicular to the planes of principal tensile stress. The shear strength of an RC beam increases as the concrete material strength increases. The tensile strength of the concrete is known to have a great influence on the shear strength, but the concrete compressive strength (f'_c) is used instead in most shear strength formulas. This approach is used because tensile tests are more difficult to conduct and usually show greater scatter than compression tests.

The shear span to depth ratio (a/d) does not considerably affect the diagonal cracking for values larger than 2.5. The shear capacity increases as the shear span to depth ratio decreases. This phenomenon is quite significant in deep beams ($a/d \leq 2.5$) because a portion of shear is transmitted directly to the support by an inclined strut or

arch action. For deep beams, the initial diagonal cracking develops suddenly along almost the entire length of the test region (Wight and MacGregor, 2009).

3.3. BASIC SHEAR TRANSFER MECHANISMS

The 1973 ASCE-ACI Committee 426 Report concluded that shear is transferred by the following four mechanisms: shear stress in the uncracked concrete, interface shear transfer, dowel action, and arch action. In a RC beam, after the development of flexural cracks, a certain amount of shear is carried by the concrete in the compression zone. The shear force carried by the uncracked concrete in the compression zone can be represented by the compressive strength of concrete and the longitudinal reinforcement ratio. Shear may continue to be transferred across a crack in the concrete by interface shear transfer, also known as aggregate interlock. Since the flexural crack width is approximately proportional to the strain of the tension reinforcement, the crack width at failure becomes smaller as the longitudinal reinforcement ratio is increased. It is also expected that the interlocking force will be increased when the compressive strength of the concrete is high. If longitudinal reinforcing bars cross a crack, dowel forces in the bars will resist shear displacement. The dowel force induces tension in the surrounding concrete that may produce splitting cracks along the longitudinal reinforcement. Although there is some contribution in dowel action by the number and arrangement of longitudinal bars, spacing of flexural cracks, and the concrete cover, the main factors influencing this mechanism are the flexural rigidity of the longitudinal bars and the strength of the surrounding concrete. Arch action occurs where shear flow cannot be transmitted. Arch action is dominant in deep beams. For this mechanism to be developed, a tie is required

to restrain the thrust developed as a result of the arch. For deep beams, failure is often due to anchorage failure of the bars restraining this thrust.

Shear can be carried through beam action, arch action or any combination of the two. When shear is carried through beam action, the tensile force in the reinforcement varies through bond stresses and plane sections remain plane. These are the normal assumptions of elastic beam theory.

The 1998 ASCE-ACI Committee 445 Report highlights a new mechanism, residual tensile stresses, which are transmitted directly across cracks. The basic explanation of residual tensile stresses is that when concrete first cracks, small pieces of concrete bridge the crack and continue to transmit tensile force as long as cracks do not exceed 0.00197-0.0059 in. in width. The application of fracture mechanics to shear design is based on the premise that residual tensile stress is the primary mechanism of shear transfer.

3.4. SHEAR DESIGN PRINCIPLES

3.4.1. Truss Model. The truss method of analysis has for some time been accepted as an appropriate method for the design of structural concrete members comprising both reinforced and prestressed concrete elements, and it now forms the basis of many design standard recommendations. The truss model was presented by the Swiss engineer Ritter (1899) to explain the flow of forces in cracked reinforced concrete. The principle of the truss model is based on the following assumptions: (1) the longitudinal tension reinforcement acts as a tension chord of the truss while the flexural compressive zone of the beam acts as the compression chord, and (2) the diagonal compressive

stresses (green lines in **Figure 3.1**) act as diagonal members, and the stirrups (blue lines in **Figure 3.1**) are considered as vertical tension members.

Mörsch (1902), a German engineer, pointed out that the compression diagonals do not need to extend from the top of one stirrup to the bottom of the next stirrup, and that the stirrups represent a continuous field of stresses rather than the discrete diagonal compressive struts formed by the concrete. Mörsch and Ritter neglected the tensile stress in cracked concrete assuming that only after cracking the diagonal compression stresses would remain at 45 degrees. Mörsch also proposed truss models to explain the behavior of beams detailed with bent-up longitudinal reinforcing bars. He also used the principal stress trajectories as an indication of how tensile reinforcement should be proportioned and detailed in a region where the internal stress flow is complex. **Figure 3.2** presents the model proposed by Mörsch.

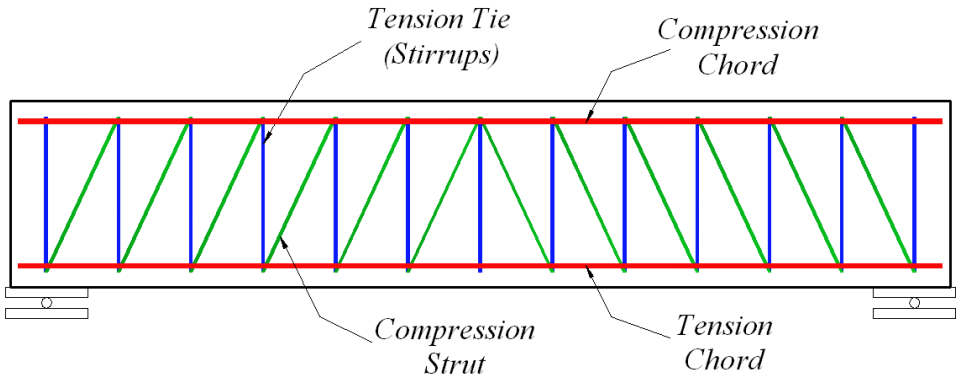

Figure 3.1: Ritter's Truss Analogy for Shear

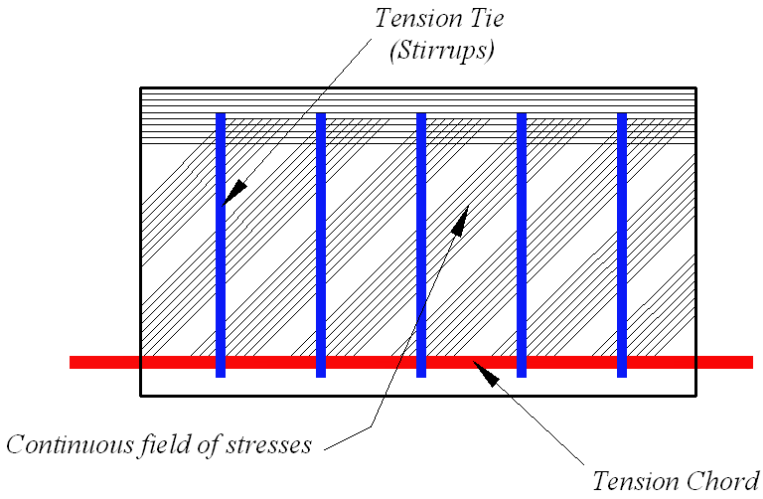

Figure 3.2: Truss Model for Beams Postulated by Mörsch

The truss model is derived using the equilibrium condition between the external and internal forces as presented in **Figure 3.3**. The shear stresses are assumed to be uniformly distributed over an effective shear area b_w wide and d deep. Between the external shear force, V, and the total diagonal compressive force, **Equation 3.1** can be written, from which the principal compressive stress (f_2) can be determined assuming a crack angle of 45 degrees.

The longitudinal component of the diagonal compressive force is considered equal to the external shear force. The tensile stress in the stirrups is determined considering **Equation 3.2**. Allowing only the use of the 45 degrees crack angle the method is robust and gives conservative results, and it is widely used by designers because of its simplicity.

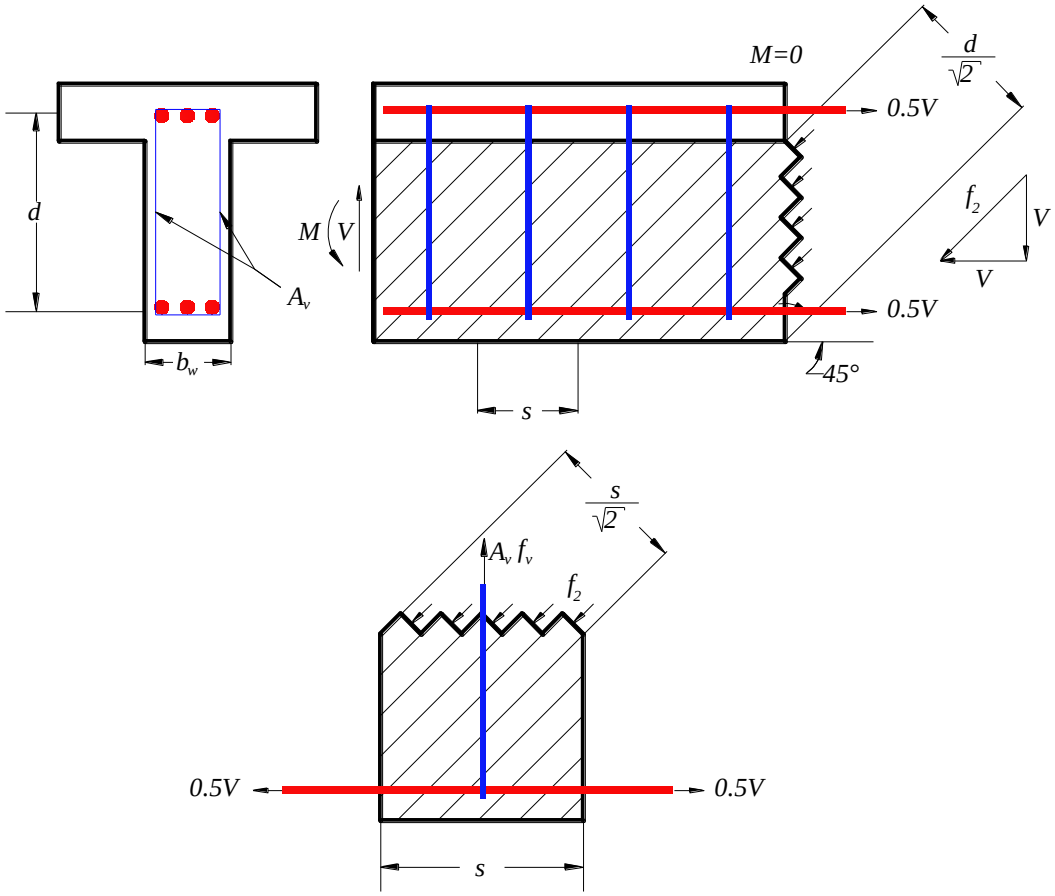

Figure 3.3: Equilibrium Conditions for the Truss Model (Collins and Mitchell, 1991)

$$\frac{f_2 b_w d}{\sqrt{2}} = \sqrt{2}V \tag{3.1}$$

$$\frac{A_v f_v}{s} = \frac{V}{d} \tag{3.2}$$

The variable-angle truss model is derived from the Mörsch truss model. This model adds a concrete contribution to shear strength to compensate for the conservative nature of the model based on a variable angle of the crack (θ). The principle is very similar to the one presented in **Figure 3.3**. In this model, the required magnitude of the principal compressive stress (f_2) is determined from the equality between the resultant of the diagonal stresses and the diagonal projection of the shear force, as stated in **Equation 3.3**. The tensile force in the longitudinal reinforcement (N_h) due to shear will be equal to

the horizontal projection of the shear force, as stated in **Equation 3.4**. The tensile stress in the stirrups is multiplied by the factor $\tan\theta$, as stated in **Equation 3.5**.

$$f_2 = \frac{V}{b_w d}(\tan\theta + \cos\theta) \tag{3.3}$$

$$N_h = V\cos\theta \tag{3.4}$$

$$\frac{A_v f_v}{s} = \frac{V}{d}\tan\theta \tag{3.5}$$

Since there are only three equations of equilibrium (**Equations 3.3**, **3.4**, and **3.5**), and there are four unknowns (f_2, N_h, f_v, and θ), the stresses in a beam caused by a given shear force cannot be explicitly determined. For design considerations, the shear force can be predicted assuming the crack angle at 45 degrees and the tensile stress in the stirrups as the tensile strength of steel (f_y). Another approach could be assuming the compressive stress in the concrete to determine the crack angle (**Equation 3.3**) and the shear force (**Equation 3.5**). Other approaches to solving the variable angle truss model have been developed based on subsequent test data. For instance, it has been suggested that the effective compressive strength should be taken as $0.6f'_c$, and that the factor $\tan\theta$ should be less than 0.5 (Collins and Mitchell, 1991).

Proportioning and detailing of the transverse reinforcement in members with a complex flow of internal stresses was a main aspect of structural concrete research in central Europe during the 1960s and 1970s. Leonhardt, from the University of Stuttgart in Germany, and Thürlimann and Müeller, from the Swiss Federal Institute of Technology in Zürich, were instrumental in the development of analysis and design methods for structural concrete regions with complex internal stress flows. Leonhardt focused mainly

on the analysis and design of deep beams and anchorage end regions in post-tensioned beams. In most of his work, the detailing of the reinforcing steel closely followed the principal tensile stress trajectories found from an elastic analysis of a homogeneous isotropic element. Thürlimann focused mainly on the application of the theory of plasticity in reinforced and prestressed concrete, with practical applications to the design for shear and torsion.

In the mid-1970s, Park and Paulay, from the University of Canterbury, extended many of the analytical and design concepts developed by Leonhardt to include, for the first time, the detailing of regions having a complex flow of stresses and subjected to cyclic load reversals caused by earthquake excitation (Park and Paulay, 1975). One of these regions is the joint between the beam and column in a moment resisting frame. In the analysis and design of beam-column joints, Park and Paulay deviated from Leonhardt's method by proposing a simple mechanism of shear transfer that did not follow the principal tensile stress trajectories shown by an elastic analysis. This model requires vertical and horizontal reinforcement to sustain the diagonal compressive field introduced into the joint as a result of bond forces from the outermost longitudinal column and beam bars.

The truss model is also the starting point of the shear friction model, also known as Loov's theory (1998), in which the shear forces are carried by stirrups and shear friction across the concrete crack. The method comprises the calculation of the shear capacity from all possible crack angles by identifying the weakest plane of failure. The force that holds the two surfaces together is equal to the yield stress multiplied by the cross-sectional area of any steel crossing the crack for bars perpendicular to the failure

plane. In addition to the friction of the failure plane surface, the model accounts for shearing of the reinforcement and the dowel action that they generate. The main drawback to the use of the shear friction models for beam shear is that the critical failure plane is typically unknown, so an interactive approach must be conducted to find the weakest or most critical failure plane.

3.4.2. Strut and Tie Model. The Strut and Tie Model (STM) was developed in the late 1980s. It was formalized and popularized by Schlaich et al. in a comprehensive paper published in 1987. Reinforced concrete theory hinges on various assumptions of simple beam theory such as plane sections remaining plane. However, regions near a discontinuity do not satisfy this assumption and are called D-regions, which stands for disturbed regions that do not follow simple beam theory. These regions extend approximately a distance *h* away from the discontinuity which may include concentrated loads, openings, or changes in the cross section. Entire beams consisting of a D-region are called deep beams. Regions in between these areas are subjected to typical beam behavior and are called B-regions. **Figure 3.4** shows the distribution of D- and B-regions, where D stands for discontinuity or disturbed, and B stands for beam or Bernoulli. The STM was developed based on the truss model to account for these D-regions. They consist of struts, ties, and nodal zones. **Figure 3.5** shows how each are combined within a beam.

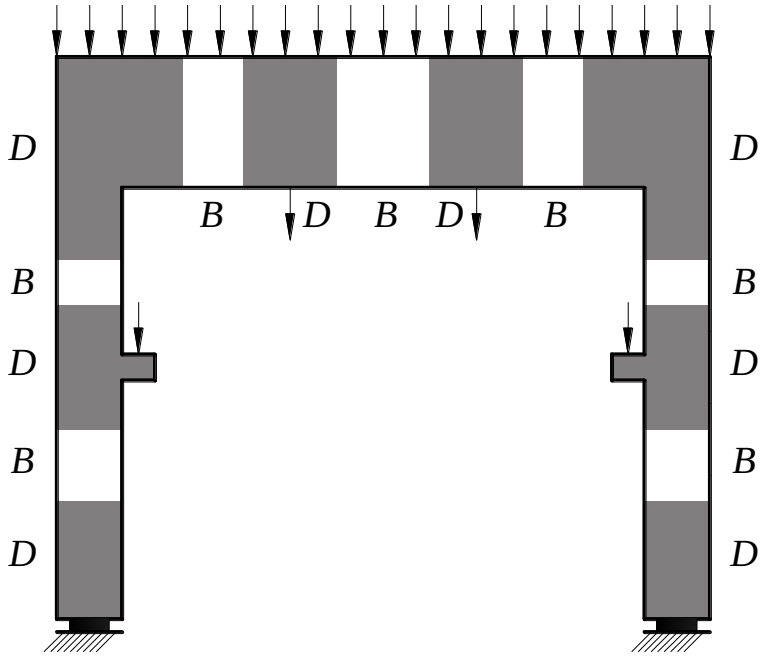

Figure 3.4: B-Regions and D-Regions (Schlaich et al., 1987)

Struts are internal concrete compression members which may be rectangular or bottle-shaped. Bottle-shaped struts swell throughout their depth, and are wider at the center than at the ends. The STM shown in **Figure 3.5** features a rectangular strut, but the bottle-shaped strut is depicted with dashed lines. Ties are tension members within the model and consist of steel reinforcement, plus the portion of concrete surrounding the steel. However, the model assumes that the steel carries all of the tension force. Nodal zones are regions where struts, ties, and concentrated loads meet. Nodes are classified by the types of forces passing into them, which create four types: (a) C-C-C, (b) C-C-T, (c) C-T-T, and (d) T-T-T, where C represents compression and T represents tension. **Figure 3.6** presents each node type.

The following procedure is used to develop a STM:

- Defining of the D-region; borders and forces within these boundaries.
- Drawing a STM based on the assumed node geometry.

- Solving for the truss member forces.
- Calculating the reinforcement layout providing the required tied capacity and enough anchorage length for the bars to ensure the correct behavior at the nodes.
- Dimensioning nodes using truss member forces obtained previously.
- Repeating analysis for the new geometry in order to find a converged solution.

The STM method is not always trouble-free and has many uncertainties. There are four major problems in developing a STM, and these are:

- Uncertainties in obtaining dimensions, stiffness, and effective strength of strut, ties, and nodes for the truss models.
- Need to select the optimal STM and iteratively adjust and refine the truss geometry.
- Need to combine different load cases.
- Multiple potential solutions for statically indeterminate models.

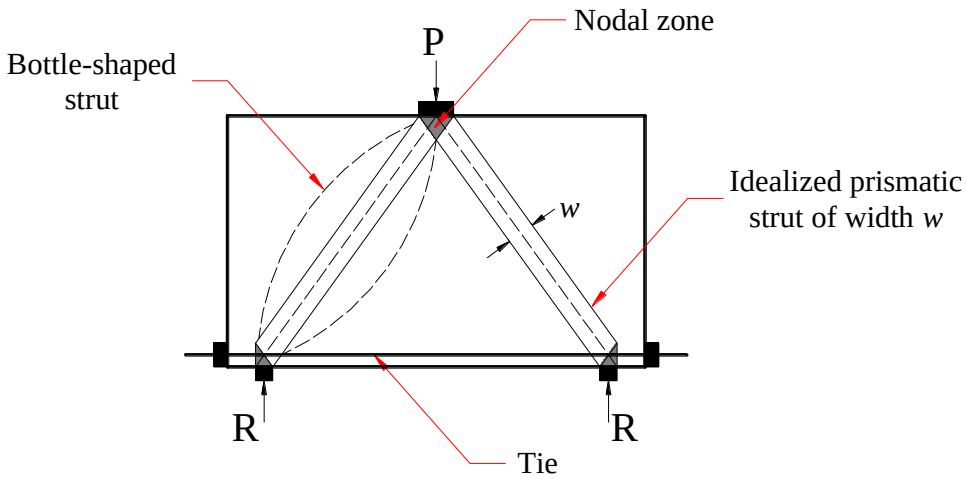

Figure 3.5: Strut and Tie Model (Nilson et al., 2004)

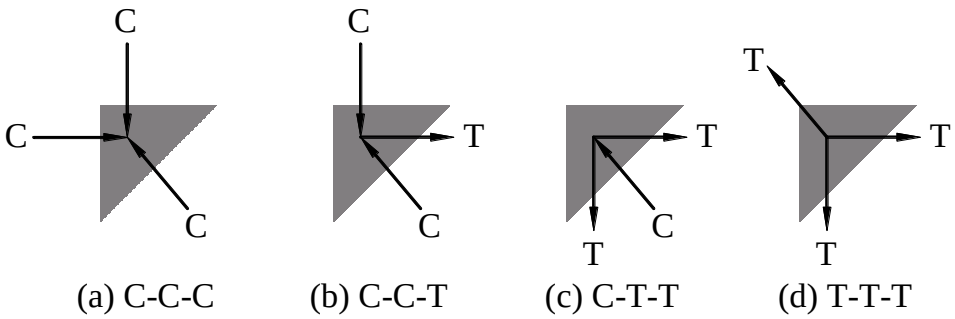

Figure 3.6: Nodal Zones (Nilson et al., 2004)

The creation of the strut and tie model offers no unique solution, and more than one admissible model may be valid for a given problem. The STM must be statically admissible, thus, in equilibrium with the external loads, reactions and nodes. Design takes place by selecting the amount of steel for the tension ties, effective width of the strut, and shape of the nodal zone such that the strength is adequate.

Previous researchers (Kani, 1967) have found that beams with shear span-to-depth ratios greater than 2.5 are governed by conditions away from the disturbed regions adjacent to the support and the loads. In this range, the strength of the beam is not influenced by details such as the size of the bearing plates, and the strength decreases by

only a small amount as the shear span increases. Collins and Mitchell (1997) presented an example of the use of the strut and tie model illustrated in **Figure 3.7**, which shows how the shear strength of a simply supported reinforced concrete beam loaded with two point loads changes as the shear span changes. This study shows that a beam can resist a higher shear force if the shear is produced by a load that is closer to the support. This series of beams was tested by Kani (1967), and based on the observation of the results, it was concluded that the shear strength was reduced by a factor of about 6 as the shear span-to-depth ratio decreased from 1 to 7 (Collins and Mitchell, 1997). This result can be explained by the fact that deep beams carry the load by strut-and-tie action, and as the applied load moves closer to the support, the angle of the compression strut increases, reducing the force (stress) in the strut, and thus increasing the capacity of a given cross section. A typical failure mode of these beams involves crushing of the concrete strut.

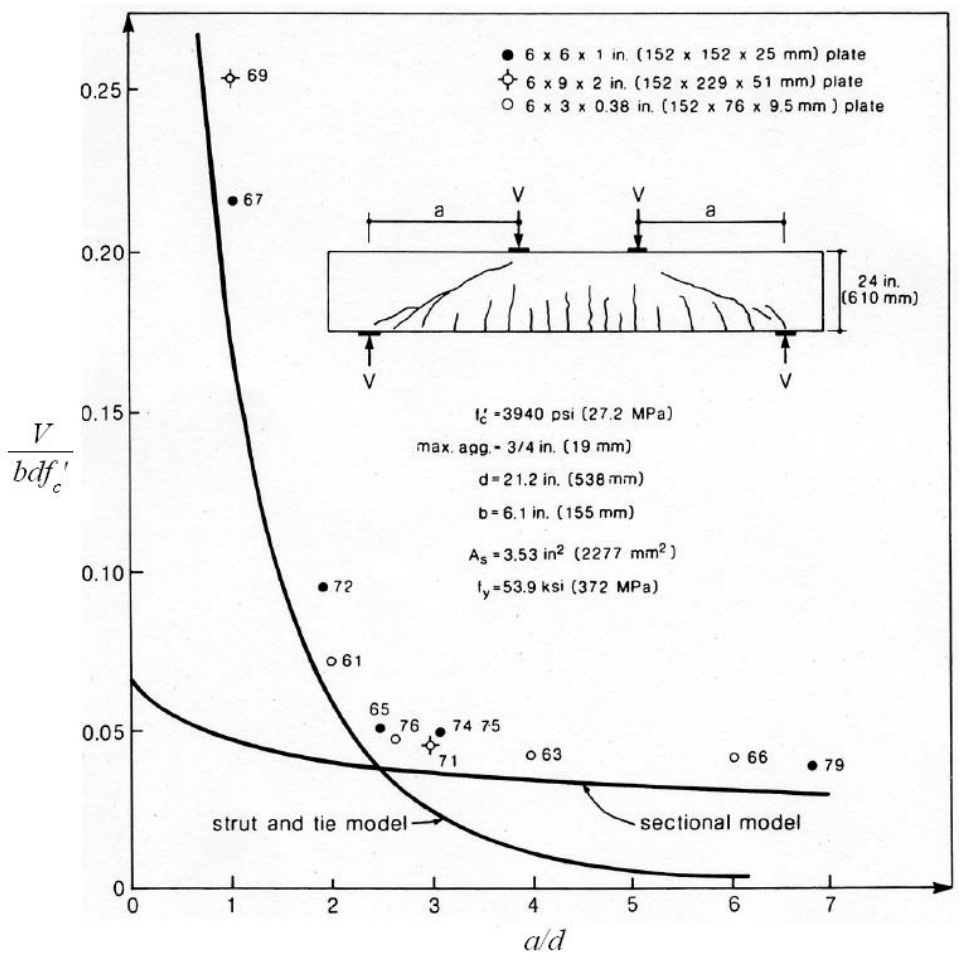

Figure 3.7: Predicted and Observed Strengths of a Series of RC Beams Tested by Kani (Collins and Mitchell, 1997)

The STM approach is rapidly gaining popularity for the analysis and design of deep beams, and has been adopted in several North American codes, such as the American Concrete Institute (ACI) Building Code Requirements for Structural Concrete (ACI 318-08) and the Canadian Standard Association (CSA) Design of Concrete Structures (CSA A23.3-04). Appendix A of ACI 318-08 provides guidance for sizing struts, nodes, and ties. The code addresses the performance of highly stressed compression zones that may be adjacent to or crossed by cracks in a member, the effect of stresses in nodal zones, and the requirements for bond and anchorage of ties. However,

ACI 318-08 provides no clear guidance to indicate when a strut should be considered as rectangular or bottle-shaped.

Furthermore, as shown in **Figure 3.8**, structural elements may consist of B-regions, D-regions, or a combination of both depending on several factors. ACI 318-08 states that if there is a B-region located between D-regions in a shear span, as shown in **Figure 3.8(b)**, the strength of the shear span is governed by the strength of the B-region if the B- and D-regions have similar geometry and reinforcement. This is because the shear strength of a B-region is less than the shear strength of a comparable D-region. Shear spans containing B-regions are designed for shear using traditional truss model approaches.

Figure 3.9 presents the layout and dimensions of the beam specimens tested in the current study. Based on the previous discussion, the presence of B-regions within the shear span precludes the application of a STM approach in determining the capacity of this section. Instead, these beams are governed by the traditional truss model approach.

3.4.3. Modified Compression Field Theory. The Modified Compression Field Theory (MCFT) was developed by Vecchio and Collins in 1986, and is a further development of the Compression Field Theory (CFT) derived by Collins and Mitchell in 1980. In the CFT it is assumed that the principal tensile stress (f_1) is zero after the concrete has cracked while in the MCFT the effect of the residual stress in the concrete between the cracks is taken into account. Tensile stresses across the diagonal struts increase from zero at the cracks to a maximum in the middle of the strut as shown in **Figure 3.10**.

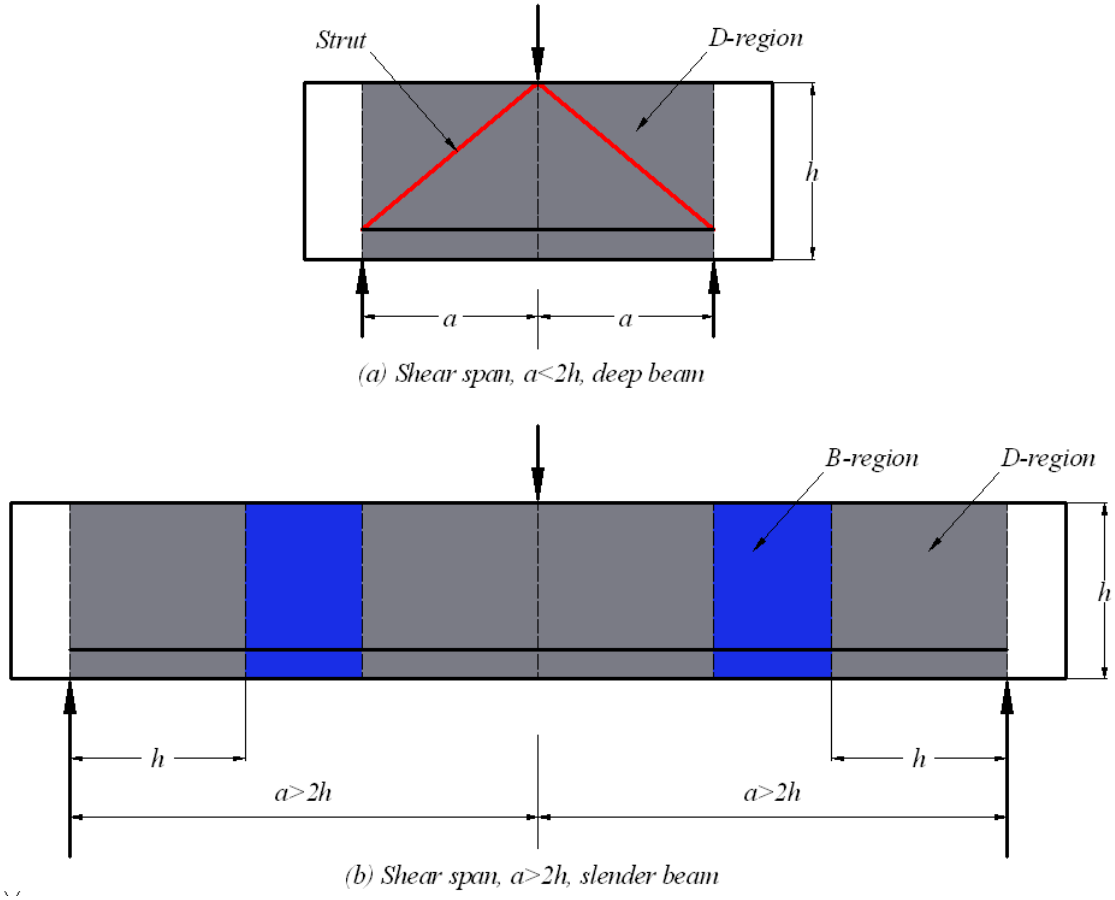

Figure 3.8: Description of Deep and Slender Beams (ACI 318-08)

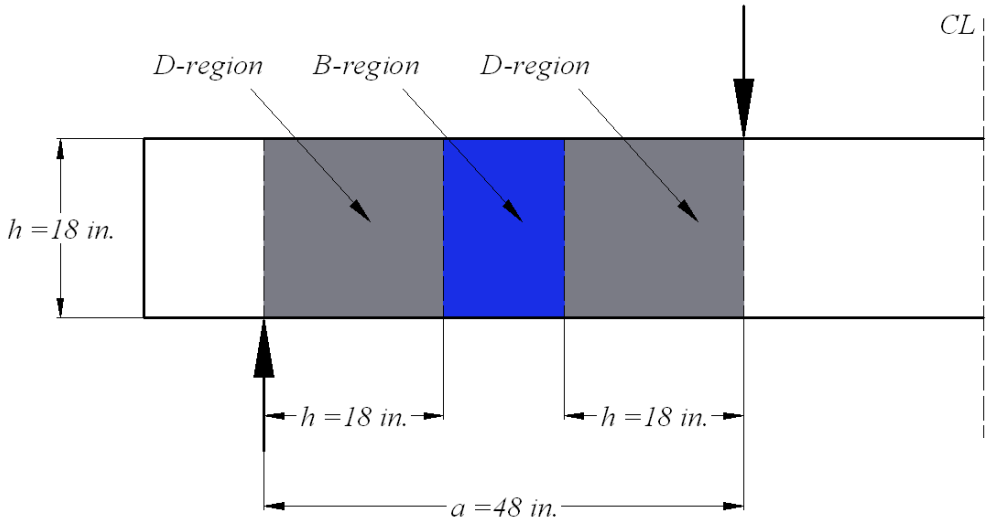

Figure 3.9: Slender Beams Used in This Study

The MCFT model consists of strain compatibility and equilibrium equations which can be used to predict the complete shear deformation response. All the compatibility equations are expressed in terms of average strains measured over base lengths long enough to include several cracks. The compatibility equations for both the CFT and the MCFT are given in **Equations 3.6**, **3.7**, and **3.8**, which are obtained from the Mohr's circle shown in **Figure 3.11**.

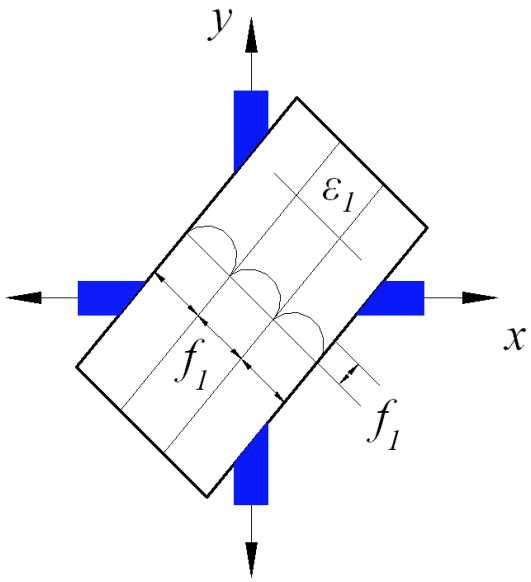

Figure 3.10: Tensile Stress Along a Cracked Strut (Vecchio and Collins, 1986)

$$\gamma_{xy} = \frac{2(\varepsilon_x - \varepsilon_2)}{\tan\theta} \tag{3.6}$$

$$\varepsilon_1 + \varepsilon_2 = \varepsilon_x + \varepsilon_y \tag{3.7}$$

$$tan^2\theta = \frac{\varepsilon_x - \varepsilon_2}{\varepsilon_y - \varepsilon_2} = \frac{\varepsilon_1 - \varepsilon_y}{\varepsilon_1 - \varepsilon_x} \tag{3.8}$$

where γ_{xy} is the shear strain, ε_x is the strain in the x-direction, ε_y is the strain in the y-direction, ε_1 is the principal tensile strain in concrete (positive value), and ε_2 is the principal compressive strain in concrete (negative value).

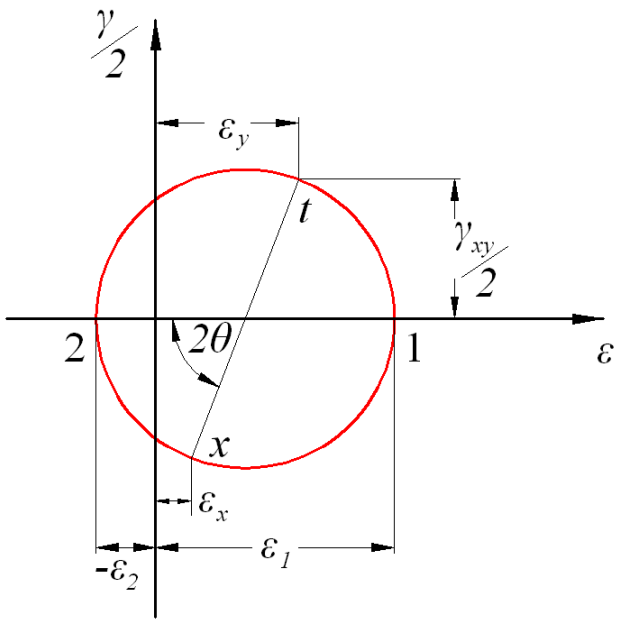

Figure 3.11: Mohr's Circle for Average Strains

The concrete element shown in **Figure 3.12** will resist concrete shear forces (v_{cxy}), horizontal concrete stresses (f_{cx}), and vertical concrete stresses (f_{cy}). All three forces combine to form the principal tensile stress (f_1), and the principal compressive stress (f_2). Converting these stresses into a Mohr's circle of stress, as shown in **Figure 3.13**, the equilibrium **Equations 3.9** and **3.10** can be derived.

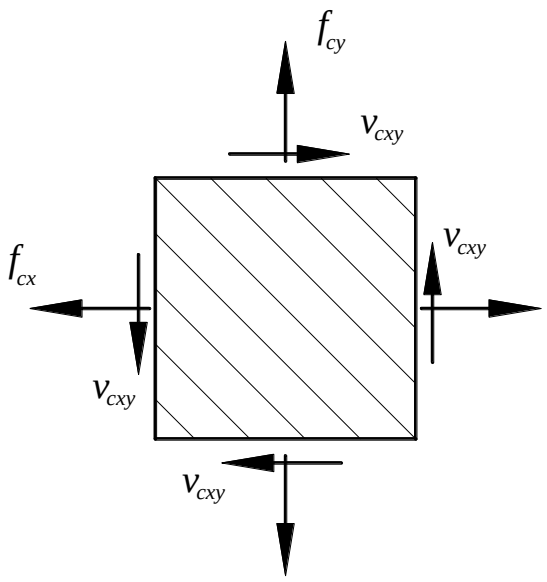

Figure 3.12: Average Concrete Stress in a Cracked Element (Vecchio and Collins, 1986)

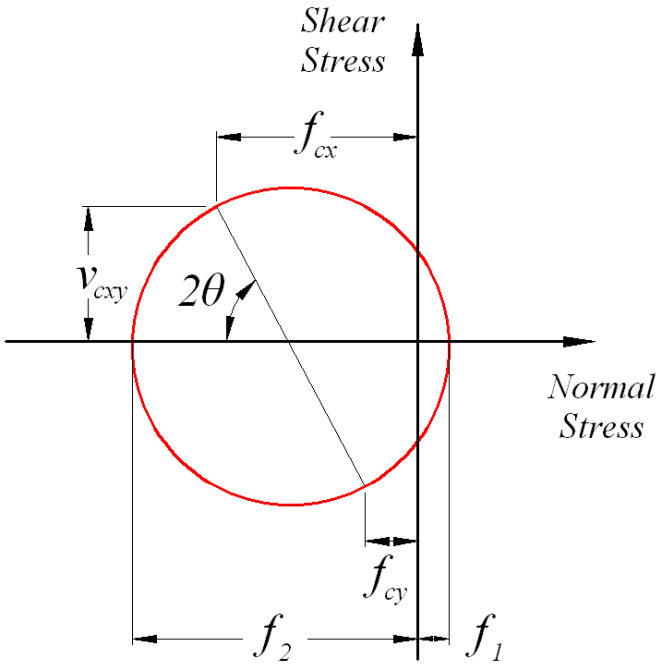

Figure 3.13: Mohr Stress Circle for Average Concrete Stresses

$$f_{cx} = f_1 - \frac{v_{cxy}}{\tan\theta} \tag{3.9}$$

$$f_{cy} = f_1 - v_{cxy}\tan\theta \tag{3.10}$$

The Mohr's circle can also be used to derive an equation for relating the principal compressive stress (f_2) and tensile stresses as shown in **Equation 3.11**.

$$f_2 = (\tan\theta + \cot\theta)v - f_1 \tag{3.11}$$

where, $v = \frac{V}{b_w jd}$ and jd is the distance between the resultants of the internal compressive and tensile forces on a cross section.

The equilibrium conditions for a symmetrical cross section subjected to pure shear are shown in **Figure 3.14**. These conditions can be expressed as shown in **Equation 3.12**.

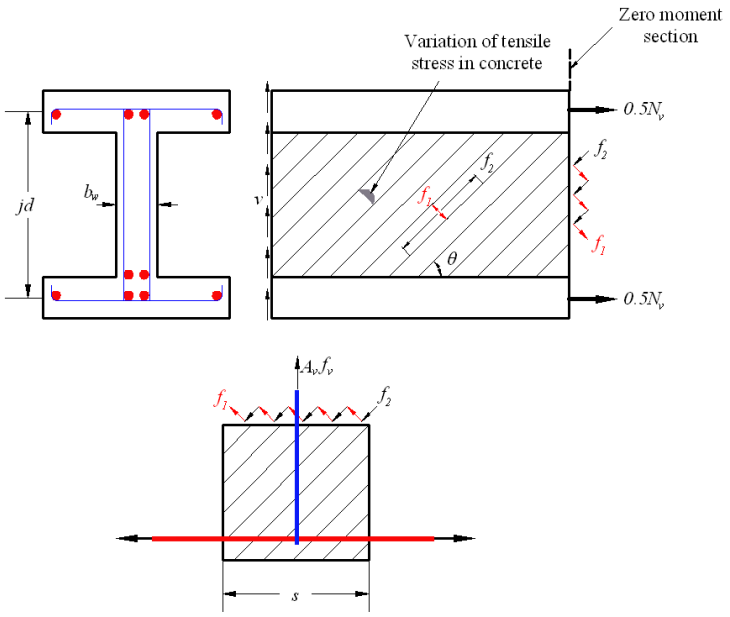

Figure 3.14: Cross Section, Principal Stresses, and Tension in Web Reinforcement (Collins and Mitchell, 1991)

$$A_v f_v = (f_2 sin^2\theta - f_1 cos^2\theta) b_w s \quad (3.12)$$

where A_v is the steel vertical reinforcement area and f_v is the stress in the stirrups. Substituting **Equation 3.11** into **3.12** generates the expression in **Equation 3.13**.

$$V = f_1 b_w jd \cot\theta + \frac{A_v f_v}{s} jd \cot\theta \quad (3.13)$$

Collins and Mitchell (1991) noted that **Equation 3.13** expresses shear resistance in terms of the sum of the concrete and steel contributions, as the traditional or classical method. The concrete contribution depends on the average tensile stresses in the concrete, and the steel contribution depends on the tensile stresses in the stirrups. It must be clarified that although the MCFT and the truss model approaches might seem to be similar, the concrete contribution from the concrete suggested by the MCFT is not constant as assumed in the classical truss model. The shear contribution of the concrete (V_c) in the MCFT is not equal to the shear strength of a similar member without shear reinforcement. According to the MCFT, the contribution of the concrete is a function primarily of the crack width. Increasing the number of stirrups reduces the crack spacing, this decreases the crack width and thus increases the concrete contribution (Cladera, 2002).

One of the most important features of the MCFT is the average strain-stress relationships derived from the tests of reinforced panels subjected to pure shear (Vecchio and Collins, 1986). The concrete compressive strength is reduced to take into account softening due to transverse tensile strain (ε_1). Initially, a parabolic relationship for

cracked concrete in compression subjected to high tensile strains in the direction normal to the compression was suggested, as shown in **Equation 3.14**.

$$f_2 = f_{2,max}\left[2\left(\frac{\varepsilon_2}{\varepsilon'_c}\right) - \left(\frac{\varepsilon_2}{\varepsilon'_c}\right)^2\right] \tag{3.14}$$

where ε'_c is the strain in the concrete, and for the MCFT, $\beta = \frac{f_{2,max}}{f'_c} = \frac{1}{0.8-0.34\frac{\varepsilon_1}{\varepsilon'_c}} \leq 1.0$

This relationship for the concrete softening (β) was derived for the MCFT in which the crack slip is not taken into account. According to Vecchio and Collins (1993), concrete strength can also have an influence in concrete softening. Moreover, size effects can also have an effect. For concrete in tension, the curve proposed in Vecchio and Collins (1986) is given by **Equations 3.15** and **3.16**.

$$\text{If } \varepsilon_1 \leq \varepsilon_{cr} \text{ then } f_1 = E_c\varepsilon_1 \tag{3.15}$$

$$\text{If } \varepsilon_1 > \varepsilon_{cr} \text{ then } f_1 = \frac{f_{cr}}{1+\sqrt{200\varepsilon_1}} \tag{3.16}$$

where ε_{cr} is the crack strain, E_c is the modulus of elasticity of the concrete, and f_{cr} is the stress in the concrete at cracking.

Equation 3.16 was updated by Vecchio and Collins (1993) to include two new parameters (α_1 and α_2) to account for the bond characteristics of the reinforcement and the type of loading. The updated equation is presented in **Equation 3.17**.

$$f_1 = \frac{\alpha_1 \alpha_2 f_{cr}}{1+\sqrt{500\varepsilon_1}} \quad (3.17)$$

where, $f_{cr} = 0.33\sqrt{f'_c}$

The stress and strain formulations adopted in the MCFT use average values, so local variations are not considered. In this methodology, a check must be done to ensure that the reinforcement can take the increment in tensile stress at the crack. In order to make this check, a value of the stress along the crack must be assumed. The shear transfer at the cracks by aggregate interlock action is estimated using the relationship in **Equation 3.18**. This equation was developed based on Walraven's (1980) experiments.

The MCFT can provide accurate predictions of shear strength and deformation. The first and most important assumption made in the MCFT is that of a rotating crack model in which previous cracks are assumed to be inactive. The MCFT assumes that the angles of the axes for the principal strains and principal stresses coincide (θ). The crack in which all the checks are performed is assumed to be oriented at the same angle, θ, as the compressive stress field.

$$v_{ci} = 0.18v_{ci,max} + 1.64f_{ci} - 0.82\frac{f_{ci}^2}{v_{ci,max}} \quad (3.18)$$

where, $v_{ci,max} = \frac{\sqrt{f'_c}}{0.31+\frac{24w}{a+16}}$

In the expression above, a is the maximum aggregate size in millimeters, and w is the average crack width over the crack surface which is estimated as the product of the

principal tensile strain (ε_1) and the crack spacing (s_θ). The spacing of shear cracks is considered to be dependent on the crack spacing in the longitudinal and transverse reinforcement directions. The crack spacing can be calculated by using **Equation 3.19**. In this equation s_{mx} is the average spacing of cracks perpendicular to the longitudinal reinforcement, and s_{mv} is the average spacing of cracks perpendicular to the transverse reinforcement. Finally, s_{mx} and s_{mv} are estimated using the formulas given by **Equations 3.20** and **3.21**.

$$s_\theta = \frac{1}{\frac{\sin\theta}{s_{mx}} + \frac{\cos\theta}{s_{mv}}} \tag{3.19}$$

$$s_{mx} = 2\left(c_x + \frac{s_x}{10}\right) + 0.25k_1\frac{d_{bx}}{\rho_x} \tag{3.20}$$

$$s_{mv} = 2\left(c_y + \frac{s}{10}\right) + 0.25k_1\frac{d_{bv}}{\rho_v} \tag{3.21}$$

where c_x and c_y are the concrete covers for the longitudinal and transverse reinforcement respectively; s_x and s are the spacing of the longitudinal and transverse reinforcement respectively; d_{bx} and d_{bv} are the bar diameters of the longitudinal and transverse reinforcement respectively; ρ_x and ρ_v are the ratios for the longitudinal and transverse reinforcement respectively; and k_1 equals 0.4 for deformed bars and 0.8 for plain bars.

The MCFT has been criticized from a practical perspective since it requires the use of a computer in order to solve the system of equations. This problem was addressed

by Bentz and Collins by providing two free software packages, called RESPONSE 2000 and MEMBRANE 2000, to solve these equations.

Bentz et al. (2006) developed simplified versions of the MCFT which can be used in order to predict the maximum shear capacity rather than the complete load-deformation response. **Equations 3.22** and **3.23** present these expressions that are also incorporated in the Canadian Code CSA A23.3 (2004).

$$V_r = V_c + V_s \leq 0.25 \emptyset_c f'_c b_w d_v \tag{3.22}$$

$$V_r = \emptyset_c \beta \sqrt{f'_c} b_w d + \emptyset_s \frac{A_{sw}}{s} f_y d_v \cot\theta \tag{3.23}$$

where $\emptyset_c$ and $\emptyset_s$ are the capacity reduction factors, b_w is the width of the web, d_v is the effective shear depth ($d_v = 0.9d$), A_s is the area of longitudinal reinforcement on the flexural tension side. The parameter β represents the shear retention factor that can be defined as the ability of cracked concrete to transmit shear by means of aggregate interlock, while θ is the angle of inclination of the strut. These two parameters are estimated in terms of the longitudinal strain at the mid-depth of the section using **Equations 3.24** and **3.25**.

$$\beta = \frac{0.40}{1+1500\varepsilon_x} \cdot \frac{1300}{1000+s_{xe}} \tag{3.24}$$

$$\theta = 29 + 7000\varepsilon_x \tag{3.25}$$

where, $\varepsilon_x = \frac{\frac{M_f}{d}+V_f}{2E_sA_{sl}}$

The parameters V_f and M_f are the factored shear force and moment at the section. The effective crack spacing (s_{xe}) is taken as 11.8 in. for members with at least minimum stirrups and for members without stirrups, $s_{xe} = \frac{35s_x}{15+a_g} \geq 0.85s_x$. The crack spacing parameter (s_x) is the longitudinal spacing between cracks, measured at mid-depth of the member. For members without horizontal reinforcement at the web, s_x is usually taken as d_v.

3.4.4. Fracture Mechanics Approach. Although fracture mechanics was developed by Griffith in 1920, for half a century, it was considered inappropriate for concrete. The reason that it took so long to apply this method to concrete is that the traditional fracture mechanics approach was developed for homogeneous materials, such as steel. However, the existence of a size effect observed in experimental results obtained during previous research (Bazant and Kim, 1984) prompted several researchers to apply fracture mechanics to shear failures. The use of fracture mechanics in design could increase the safety and reliability of concrete structures. Numerous analytical and numerical tools have been developed to simulate the fracture behavior of concrete structures, and in connection with these developments, researchers are focused on designing experimental methods to measure the different parameters required for these models. The ACI 446.1R (1999) document highlights five compelling reasons to use a fracture mechanics approach. The first one is the energy required for crack formation. This reason states that the actual formation of cracks requires energy, called fracture energy, which represents the surface energy of a solid. The second one is the objectivity

of the calculations. Any physical theory must be objective and the result of the calculations must not depend on subjective aspects such as choice of coordinates, mesh, etc. Objectivity should come ahead of experimental verification. The third reason is the lack of yield plateau. Based on load-deflection diagrams, there are two distinguishable basic types of structural failure, plastic and brittle. Plastic failures typically develop a single-degree-of-freedom mechanism such that the failure proceeds simultaneously in various parts of the structure. These failures are characterized by the presence of a long yield plateau on the load-deflection diagram. If this diagram does not have such a plateau, the failure is brittle or brittle-ductile. The fourth reason is capability to absorb energy, as related to ductility. The area under the complete load-deflection diagram of a concrete or reinforced concrete member represents the energy which the element will absorb during failure, and this energy must be supplied by the loads. The current plastic limit analysis cannot give information on the post-peak decline of the load and energy dissipated in this process. The fifth and most compelling reason for using fracture mechanics is the size effect. ACI 446.1R (1999) defines the size effect through a comparison of geometrically similar structures of different sizes, characterized in terms of the nominal stress at maximum ultimate load. When this nominal stress does not change its value for geometrically similar structures of different sizes, it can be said that there is no size effect.

The study of fracture mechanics of concrete started in 1961 with Kaplan. Later, in 1972, Kesler et al. concluded that the classical linear elastic fracture mechanics (LEFM) approach with only one fracture parameter, either the fracture energy or the fracture

toughness, was not applicable to concrete. Kesler et al. suggested at least two fracture parameters.

The simplest model that describes the progressive fracture process is the cohesive crack model (Hillerborg et al., 1976). Hillerborg et al. proposed the cohesive crack model for simulation of plain concrete, in which concrete fracture energy characterized the softening response of a cohesive crack that could develop anywhere in a concrete structure. The softening curve is the main feature of the cohesive crack model. This curve presents an initial portion with a steep descending slope, followed by a smooth drop when the stress reaches a value approximately equal to 1/3 of the nominal tensile strength (f'_t), and a long tail asymptotic to the horizontal axis (crack opening, *w*) as shown in **Figure 3.15**. Geometrically, the area under the complete curve represents the fracture energy. The fracture energy is defined as the amount of energy necessary to create a crack of unit surface area projected in a plane parallel to the crack direction.

Hillerborg (1985) provided a theoretical basis for a concrete fracture energy testing procedure, often referred to as the work-of-fracture method (WFM), in which the fracture energy per unit area of concrete is computed as the area under the experimental load-deflection response curve for a notched concrete beam subjected to three-point bending, divided by the area of fracture concrete.

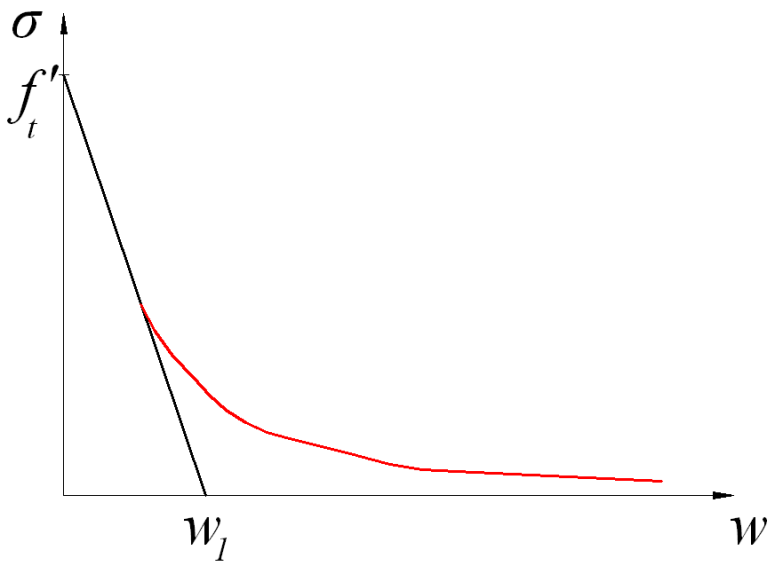

Figure 3.15: Softening Function and Initial Tangent for Cohesive Crack Model (Einsfeld and Velasco, 2006)

For example, when conducting three-point bending tests on notched beams, as the beam splits into two halves, the fracture energy (G_F) can be determined by dividing the total dissipated energy by the total surface area of the crack as shown in **Equation 3.26**.

$$G_F = \frac{W}{b(d-a_0)} \tag{3.26}$$

where W is the total energy dissipated in the test, and b, d, and a_0 are the thickness, height and notch depth of the beam, respectively.

Several additional test methods have been proposed in recent years to determine concrete fracture properties from which fracture energy may be computed.

In 1987, Bazant and Pfeiffer concluded that the cohesive crack model results in fracture characteristics that are ambiguous and size-dependent. As a consequence, different values for the fracture energy could be obtained for specimens of different sizes.

Bazant and Pfeiffer proposed a method where the fracture energy is calculated based on the size effect law. In this approach, the fracture energy is independent of the size of the specimens. This asymptotic approach is known as the size effect method (SEM). Bazant and Pfeiffer suggested the following relationship shown in **Equation 3.27**.

$$\sigma_N = B(1 + \beta^k)^{\frac{1}{2k}} \tag{3.27}$$

where σ_N is the nominal stress at failure, B is the coefficient obtained through the linear regression plot of the results, β is the brittleness number, and k is a parameter to reflect the size effect.

The brittleness number indicates whether the behavior of any structure is related to either the limit state analysis or to LEFM analysis. Bazant and Pfeiffer proposed **Equation 3.28** for the brittleness number.

$$\beta = \frac{d}{d_0} \tag{3.28}$$

where d is the characteristic dimension of the structure (for their study, the specimen height), and d_0 is a coefficient determined experimentally. The coefficients B and d_0 are determined by linear regression. In this approach, specimens of different sizes but geometrically similar can be rearranged in a linear regression plot as shown in **Equation 3.29**. **Equations 3.30** to **3.33** present the different relationships for the parameters contained in **Equation 3.29**.

Rupture of a structure of infinite size follows the LEFM theory, since the plastic region around the concrete fracture zone is relatively small. In this case, the fracture energy can be calculated using **Equation 3.34**.

$$y = Ax + C \tag{3.29}$$

$$y = \left(\frac{1}{\sigma_N}\right)^2 \tag{3.30}$$

$$x = d \tag{3.31}$$

$$d_0 = \frac{C}{A} \tag{3.32}$$

$$B = \frac{1}{\sqrt{C}} \tag{3.33}$$

$$G_f = \frac{g_f(\alpha_0)}{AE} \tag{3.34}$$

where E is the modulus of elasticity of the concrete, A is the angular coefficient of the linear regression plot, $g_f(\alpha_0)$ is the non-dimensional energy release rate calculated according to LEFM, and α_0 is the relative notch length defined in **Equation 3.35**.

$$\alpha_0 = \frac{a_0}{d} \tag{3.35}$$

The fracture energy normally associated with WFM is different from the one calculated through SEM. They are usually differentiated as G_F for values calculated with WFM, and G_f for values calculated using SEM. The values obtained with WFM are

sensitive to the specimen size and shape. On the other hand, values obtained with SEM are independent of the structure size as well as geometry (Einsfeld and Velasco, 2006).

While G_F corresponds to the area under the complete softening stress-separation curve of the cohesive crack model, G_f corresponds to the area under the initial tangent of the stress-separation curve as shown in **Figure 3.16**.

Bazant and Kim (1984) and Bazant and Sun (1987) developed a set of equations to describe the dependence of the diagonal shear strength on the size, shape, and longitudinal reinforcement ratio of beams failing in diagonal shear. The shear strength in this model is assumed to result from the combination of the arching action and the composite beam action. The summation of the two components resulted in an expression similar to that of the ACI building code. However, this expression failed to explain the structural behavior.

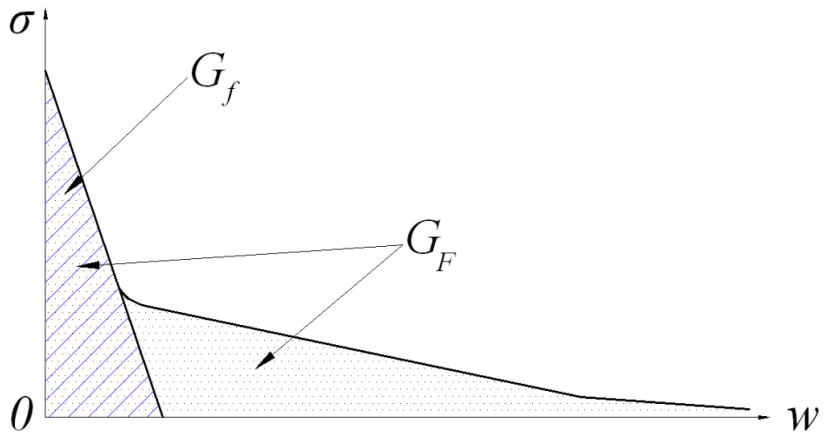

Figure 3.16: Softening Stress-Separation Curve of Cohesive Crack Model (Bazant and Becq-Giraudon, 2002)

Gustafsson and Hillerborg in 1988 investigated the diagonal shear strength of members without stirrups using the cohesive crack concept, with the objective to show that a size effect can be predicted theoretically. This model assumes that a single

polygonal cohesive crack with linear softening is formed, while the bulk of the concrete remains linear elastic. The behavior of the steel is assumed to be linear elastic. The failure criterion adopted is crushing of the concrete. Using this approach Gustafsson and Hillerborg analyzed the influence of the size, longitudinal reinforcement ratio, and the shear span-to-depth ratio.

Jenq and Shah (1989) adopted a more physical approach applying a two-parameter nonlinear fracture mechanics model to the shear failure. In this model, the ultimate shear capacity is assumed to be the summation of the contributions from the reinforcement and the concrete. The concrete contribution is derived using the fracture mechanics model. The steel contribution is estimated by considering the average ultimate bond stress, which is assumed to be proportional to the embedded length.

In 1993, So and Karihaloo criticized Jenq and Shah's approach pointing out that their approach was oversimplified and ignored the influence of the reinforcement on the fracture behavior of the concrete. Large discrepancies between the predicted and measured capacities confirmed their criticism. Khariloo introduced a failure criterion for longitudinal splitting using Van der Veen's model (Van der Veen, 1990) to derive the maximum bond stress. Finally, Karihaloo concluded that the bond-slip relationship, the dowel action, and the aggregate interlock must be taken into account to accurately predict the shear capacity using Jenq and Shah's approach. The only weak point of Karihaloo's model is the significant use of empirical equations.

In 2001, Gastebled and May proposed a fracture mechanics model for the flexural-shear failure of reinforced concrete beams without stirrups. This model was developed assuming that the ultimate shear load is reached when the splitting crack starts

to propagate. The critical load is calculated considering the energy balance of the system during splitting crack propagation. The position of the critical diagonal crack is obtained using Kim and White's semi-empirical formula proposed in 1991. Gastebled and May used the empirical formula for the assessment of the fracture energy proposed by the CEB-FIP Model Code.

The formulation of this model is based on the fundamental relation of LEFM presented in **Equation 3.36**, where *G* is the fracture energy consumption and W_{ext} is the work of the external force. The external load is produced by the rotation under constant load about the tip of the diagonal crack. In order to calculate the energy release, the rotational stiffness of the beam must be determined. This stiffness depends on the axial and dowel stiffness of the longitudinal reinforcement. The stiffness is calculated based on the free body diagram (FBD) presented in **Figure 3.17**.

$$\delta G = \frac{1}{2}\delta W_{ext} \tag{3.36}$$

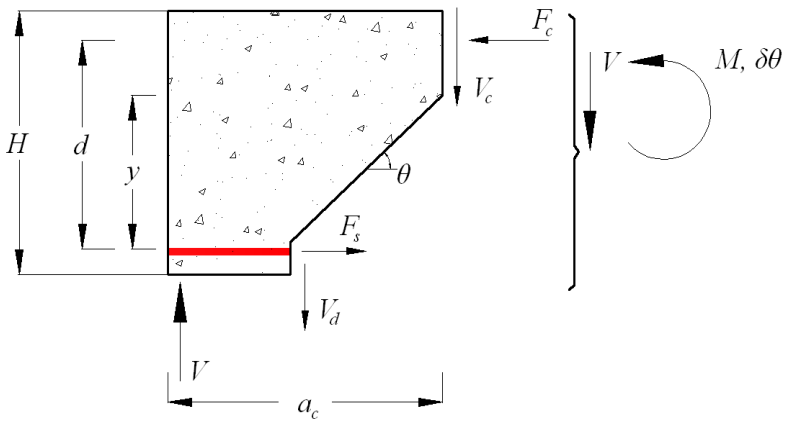

Figure 3.17: Free Body Diagram and Notation Definition (Gastebled and May, 2001)

The axial and shear force in the steel bar crossing the diagonal crack were linked to the angle of rotation (θ) using the elastic properties of the bar and the geometry of the deformation mechanism as shown in **Equation 3.37**. The beam bending theory for a circular cross section is also used to derive the dowel force as shown in **Equation 3.38**.

$$F_s = \frac{E_s A_s}{\delta_s} y\theta \tag{3.37}$$

$$V_d = \frac{G_s \Sigma_s}{\delta_s} y\theta = \frac{9}{26} \cdot \frac{E_s A_s}{\delta_s} y\theta \tag{3.38}$$

where F_s is the longitudinal reinforcement force, δ_s is the unbounded length of the reinforcement, y is the diagonal crack extent, θ is the rotation, V_d is the longitudinal reinforcement dowel force, G_s is the shear modulus of steel, and Σ_s is the reduced cross section of the bar (taken as $0.9A_s$).

The equilibrium of the FBD presented in **Figure 3.17** is reached when the following relationships shown in **Equations 3.39** to **3.41** are maintained (horizontal, vertical, and moment equilibrium, respectively). Assuming that the diagonal crack extent and the internal moment arm (jd) are proportional to the height of the beam as shown in **Equations 3.42** and **3.43**, **Equation 3.41** can be rewritten and is presented in **Equation 3.44**. **Equation 3.44** provides the rotational stiffness.

$$F_s = F_c \tag{3.39}$$

$$V_c + V_d = V \tag{3.40}$$

$$F_s jd + V_d y = V a_c \tag{3.41}$$

$$y = \beta H \tag{3.42}$$

$$jd = \gamma H \tag{3.43}$$

$$\beta\left(\frac{9}{26}\beta + \gamma\right)\frac{E_S A_S}{\delta_s} H^2\theta = V a_c \tag{3.44}$$

After differentiating **Equation 3.44** and using the fundamental relation of fracture mechanics as a criterion for splitting failure as shown in **Equation 3.36**, **Equations 3.45** and **3.46** are derived to obtain the expression for the critical shear load.

$$a_c V_{cr} \delta\theta = 2\Gamma\delta_e \tag{3.45}$$

$$V_{cr} = \sqrt{\frac{9}{13} + 2\frac{\gamma}{\beta}} \cdot \frac{\beta H}{a_c} \cdot \sqrt{\Gamma A_s E_s} \tag{3.46}$$

where δ_e is the variation of the unbonded length, and Γ is the fracture energy necessary to extend the splitting crack by a unit length. For simplicity of calculations and based on experimental observations, γ and β can be taken as 0.9 and 0.8 respectively. The units for this model have been set as follows: V_{cr} in kN, Γ in kN-m/m, A_s in mm^2, and E_s in GPa.

This model uses the equation given by the CEB-FIP Model Code for the assessment of the fracture energy and is presented in **Equation 3.47**. The maximum aggregate size (d_{agg}) is assumed in Gastebled and May's model as 0.75 in. Based on all

the previous assumptions and assuming a dynamic mode of failure, **Equation 3.46** can be simplified and is presented in **Equation 3.48**.

$$G_f = \left(0.0469 d_{agg}^2 - 0.5 d_{agg} + 26\right)\left(\frac{f'_c}{10}\right)^{0.7} \tag{3.47}$$

$$V_{cr} = 4.517 \cdot \frac{H}{a_c} \cdot (f'_c)^{0.35} \sqrt{A_s E_s b} \tag{3.48}$$

The units for this model have been set as follows: V_{cr} in kN, f'_c in MPa, A_s in m^2, and E_s in GPa, and b in mm.

The only problem in this model is the determination of the location of the critical diagonal crack. Kim and White (1991) postulated the same failure mechanism and adopted a mixed approach, partly physical and partly empirical, to predict the flexural-shear cracking and the position of the critical diagonal crack. **Equation 3.49** presents the model to calculate the location of the critical diagonal crack.

$$a_c = k_3 a_s \left(\frac{\rho_s \left(\frac{d}{a_s}\right)^2}{\left(1 - \sqrt{\rho_s}\right)^2}\right)^{\frac{1}{3}} \tag{3.49}$$

where k_3 is an empirical coefficient determined through statistical analysis and has a value of 3.3, a_s is the shear span, ρ_s is the geometrical reinforcement ratio, and d is the effective depth of the beam. Limited experimental data was available to check the position of the critical diagonal crack, however, Kim and White found 14 experimental results to perform the statistical analysis and determine a value for the coefficient k_3. Significant scatter was reported by the authors.

The final expression is obtained by substituting **Equation 3.49** into **Equation 3.48** and is shown in **Equation 3.50**. In this expression, the first term corresponds to the size effect, the second term takes into account the slenderness of the beam, the third and fourth terms reflect the reinforcement ratio influence, and the fifth term corresponds to the influence of the concrete strength.

$$V_{cr} = \frac{1.109}{\sqrt{H}} \cdot \left(\frac{H}{a_s}\right)^{\frac{1}{3}} \cdot \left(1 - \sqrt{\rho_s}\right)^{\frac{2}{3}} \cdot \rho_s^{\frac{1}{6}} \cdot f'^{0.35}_c \cdot \sqrt{E_s} \cdot bH \tag{3.50}$$

where H is the height of the beam, a_s is the shear span, ρ_s is the geometrical reinforcement ratio, f'_c is the concrete compressive strength, E_s is the steel modulus of elasticity, and b is the width of the beam.

Bazant and Becq-Giraudon (2002) formulated the empirical expression shown in **Equation 3.51** to compute fracture energy for specimens with rounded aggregate. This equation was calibrated using 161 RILEM work-of-fracture tests whereas the equation proposed by CEB-FIP was calibrated using much less data. Bazant and Becq-Giraudon also reported that G_F data computed from work-of-fracture testing have significantly more scatter than G_f data computed using other test methods and suggested that this scatter was due to errors in measurement of the tail of the load-displacement response curve.

$$G_f = 0.0143\alpha_0 \left(\frac{f'_c}{8.41}\right)^{0.40} \left(1 + \frac{D_{max}}{0.0763}\right)^{0.43} \left(\frac{w}{c}\right)^{-0.18} \tag{3.51}$$

where α_0 is an aggregate shape factor ($\alpha_0 = 1$ for rounded aggregate, and $\alpha_0 = 1.12$ for angular aggregate), f'_c is the compressive strength of the concrete, D_{max} is the

maximum aggregate size, and $\frac{w}{c}$ is the water-to-cement ratio of the concrete. The units of this model have been set as follows: f'_c in psi, and D_{max} in inches.

3.4.5. Truss Model and Modified Compression Field Theory Comparison. The MCFT can be explained as a truss model in which the shear strength is the sum of the steel and concrete contributions. The main difference from a classic truss model with concrete contribution is that the concrete contribution in the MCFT is the vertical component of the shear stress transferred across the crack (v_{ci}) and not the diagonal cracking strength.

Cladera (2002) highlighted the main differences between the truss model and the MCFT concrete contributions:

- The truss model concrete contribution is considered equal to the shear strength of a similar beam without shear reinforcement. The MCFT takes into account a concrete contribution based on the actual collapse mechanism of a RC beam.
- The truss model concrete contribution does not vary with the amount of the transverse reinforcement. The MCFT concrete contribution depends on the crack width. The more shear reinforcement, the smaller the crack width, and the greater the concrete contribution.

3.4.6. Summary of Shear Design. Shear design in structural concrete has been a challenging topic for many years. The truss analogy first proposed by Ritter (1899) and then improved by Mörsch (1902) has been a powerful tool in understanding the shear transfer mechanism in a RC beam. However, progress has been made since those early truss models. Three different groups of approaches have been developed: (1) 45 degrees

truss model, (2) compression field theories, and (3) fracture mechanics approaches. Predictions of the shear provided by these approaches have improved considerably from early formulations, which were based on empirical results. As reported by Collins et al. (2008), early design equations for shear have been proven to be unsafe since the experimental data used in calibrating the models corresponded to rather small specimens. The MCFT offers a rational approach in which the shear transmitted along the crack is limited according to the crack width and aggregate size. The STM which was developed by Schaich et al. (1987) is often claimed as a transparent method for designing and detailing discontinuity regions. It has been highlighted that the method requires several simplifications regarding geometry assumed for the truss elements or the effective strength of the struts. Finally, it is clear that several difficulties can be faced in developing a STM, such as uniqueness of the model, combinations with other load cases or dealing with statically indeterminate systems.

3.5. DESIGN CODES REVIEW

There are a variety of design code philosophies that can be found around the world for shear design. Some of these rely on empirical formulas for estimating the shear strength, such as the ACI 318-08 (2008), while others such as the AASHTO LRFD (2010) rely more on concrete models such as the MCFT. This section will detail three selected design codes.

3.5.1. American Concrete Institute, ACI 318-08. The ACI 318-08 method is most commonly used for shear design in the United States, and is based on a 45 degree truss model. The shear strength is based on an average shear stress distribution across the

entire cross section, and is composed of a concrete component (V_c) and a steel component (V_s). The basic equations for normal-weight, non-prestressed reinforced concrete are listed in **Equations 3.52** to **3.56**.

$$V_u \leq \emptyset V_n = \emptyset(V_c + V_s) \tag{3.52}$$

$$V_c = \left(1.9\sqrt{f'_c} + 2500\rho_w \frac{V_u d}{M_u}\right) b_w d \leq 3.5\sqrt{f'_c} b_w d \tag{3.53}$$

$$\text{Simplified version: } V_c = 2\sqrt{f'_c} b_w d \tag{3.54}$$

$$A_{v,min} = 0.75\sqrt{f'_c}\frac{b_w s}{f_{yt}} \geq 50\frac{b_w s}{f_{yt}} \tag{3.55}$$

$$V_s = \frac{A_v f_{yt} d}{s} \tag{3.56}$$

where, V_u is the factored shear force on the section, $\emptyset$ is the strength reduction factor equal to 0.75, V_n is the nominal shear strength, $\rho_w = \frac{A_s}{b_w d}$, A_s is the area of longitudinal reinforcement, b_w is the width of the web, d is the distance from the extreme compression fiber to the center of gravity of the steel, M_u is the factored moment at the section, f'_c is the concrete compressive strength (psi), f_{yt} is the yield strength of the transverse reinforcement (psi), s is the spacing of the transverse reinforcement, and A_v is the area of shear reinforcement. The following condition must be maintained $\frac{V_u d}{M_u} \leq 1.0$.

The ACI 318-08 presents a procedure for calculating the failure shear strength for concrete beams without shear reinforcement. The simplified method is presented in **Equation 3.54**. Some research data indicate that **Equation 3.53** overestimates the

influence of f'_c and underestimates the influence of ρ_w and $\frac{V_u d}{M_u}$. This is why, for most designs, it is convenient to assume that the second term of this equation equals to $0.1\sqrt{f'_c}$ and use **Equation 3.54** to calculate the shear contribution of the concrete.

3.5.2. AASHTO LRFD Bridge Design Specifications. The AASHTO LRFD (2010) method is known as the Sectional Design Model, and is based on the MCFT. The nominal shear resistance (V_n) can be computed by **Equations 3.57** to **3.61**.

$$V_n = V_c + V_s + V_p \tag{3.57}$$

$$V_{n,max} = 0.25 f'_c b_v d_v + V_p \tag{3.58}$$

$$V_c = 0.0316 \beta \sqrt{f'_c} b_v d_v \tag{3.59}$$

$$V_s = \frac{A_v f_y d_v \cot\theta}{s} \tag{3.60}$$

$$A_{v,min} \geq 0.0316 \sqrt{f'_c} \frac{b_v s}{f_y} \tag{3.61}$$

where, V_p is the vertical component of the prestressing force, b_v is the effective width of the web taken as the minimum web width within the depth, d_v is the effective shear depth taken as the greater of $0.9d$ or $0.72h$, β is the factor indicating the ability of diagonal cracked concrete to transmit tension, θ is the angle of inclination of the diagonal compressive struts, f'_c is the concrete compressive strength (ksi), and f_y is the yield strength of the transverse reinforcement (ksi).

For sections containing at least the minimum amount of transverse reinforcement, the values of β and θ may be found using **Table 3.1**. The designer selects the row

corresponding to the shear design stress ratio $\frac{v}{f'_c} = \frac{V_u}{b_v d_v f'_c}$, and selects the column corresponding to the longitudinal strain (ε_x) at mid-depth. The longitudinal strain may be computed using **Equation 3.62**.

Table 3.1: Values of θ and β for Sections With Transverse Reinforcement (AASHTO LRFD, 2010)

$\frac{v_u}{f'_c}$		$\varepsilon_x \times 1000$										
		≤ -0.20	**≤ -0.10**	**≤ -0.05**	**≤0**	**≤0.125**	**≤0.25**	**≤0.50**	**≤0.75**	**≤1.00**	**≤1.50**	**≤2.00**
≤0.075	θ	22.3°	20.4°	21.0°	21.8°	24.3°	26.6°	30.5°	33.7°	36.4°	40.8°	43.9°
	β	6.32	4.75	4.10	3.75	3.24	2.94	2.59	2.38	2.23	1.95	1.67
≤0.100	θ	18.1°	20.4°	21.4°	22.5°	24.9°	27.1°	30.8°	34.0°	36.7°	40.8°	43.1°
	β	3.79	3.38	3.24	3.14	2.91	2.75	2.50	2.32	2.18	1.93	1.69
≤0.125	θ	19.9°	21.9°	22.8°	23.7°	25.9°	27.9°	31.4°	34.4°	37.0°	41.0°	43.2°
	β	3.18	2.99	2.94	2.87	2.74	2.62	2.42	2.26	2.13	1.90	1.67
≤0.150	θ	21.6°	23.3°	24.2°	25.0°	26.9°	28.8°	32.1°	34.9°	37.3°	40.5°	42.8°
	β	2.88	2.79	2.78	2.72	2.60	2.52	2.36	2.21	2.08	1.82	1.61
≤0.175	θ	23.2°	24.7°	25.5°	26.2°	28.0°	29.7°	32.7°	35.2°	36.8°	39.7°	42.2°
	β	2.73	2.66	2.65	2.60	2.52	2.44	2.28	2.14	1.96	1.71	1.54
≤0.200	θ	24.7°	26.1°	26.7°	27.4°	29.0°	30.6°	32.8°	34.5°	36.1°	39.2°	41.7°
	β	2.63	2.59	2.52	2.51	2.43	2.37	2.14	1.94	1.79	1.61	1.47
≤0.225	θ	26.1°	27.3°	27.9°	28.5°	30.0°	30.8°	32.3°	34.0°	35.7°	38.8°	41.4°
	β	2.53	2.45	2.42	2.40	2.34	2.14	1.86	1.73	1.64	1.51	1.39
≤0.250	θ	27.5°	28.6°	29.1°	29.7°	30.6°	31.3°	32.8°	34.3°	35.8°	38.6°	41.2°
	β	2.39	2.39	2.33	2.33	2.12	1.93	1.70	1.58	1.50	1.38	1.29

$$\varepsilon_x = \frac{\frac{M_u}{d_v} + 0.5N_u + 0.5(V_u - V_p)\cot\theta - A_{ps}f_{po}}{2(E_s A_s + E_p A_p)} \quad (3.62)$$

For sections containing less than the minimum amount of transverse reinforcement, the values of β and θ may be found using **Table 3.2**. The designer selects the row corresponding to an equivalent spacing parameter (s_{xe}), and selects the column corresponding to the longitudinal strain at mid-depth. The equivalent spacing may be

computed using **Equation 3.63**. The longitudinal strain for this case may be computed using **Equation 3.64**.

Table 3.2: Values of θ and β for Sections With Less Than Minimum Transverse Reinforcement (AASHTO LRFD, 2010)

s_{xe} (in.)		$\varepsilon_x \times 1000$										
		≤ -0.20	≤ -0.10	≤ -0.05	≤0	≤0.125	≤0.25	≤0.50	≤0.75	≤1.00	≤1.50	≤2.00
≤ 5	θ	25.4°	25.5°	25.9°	26.4°	27.7°	28.9°	30.9°	32.4°	33.7°	35.6°	37.2°
	β	6.36	6.06	5.56	5.15	4.41	3.91	3.26	2.86	2.58	2.21	1.96
≤ 10	θ	27.6°	27.6°	28.3°	29.3°	31.6°	33.5°	36.3°	38.4°	40.1°	42.7°	44.7°
	β	5.78	5.78	5.38	4.89	4.05	3.52	2.88	2.50	2.23	1.88	1.65
≤ 15	θ	29.5°	29.5°	29.7°	31.1°	34.1°	36.5°	39.9°	42.4°	44.4°	47.4°	49.7°
	β	5.34	5.34	5.27	4.73	3.82	3.28	2.64	2.26	2.01	1.68	1.46
≤ 20	θ	31.2°	31.2°	31.2°	32.3°	36.0°	38.8°	42.7°	45.5°	47.6°	50.9°	53.4°
	β	4.99	4.99	4.99	4.61	3.65	3.09	2.46	2.09	1.85	1.52	1.31
≤ 30	θ	34.1°	34.1°	34.1°	34.2°	38.9°	42.3°	46.9°	50.1°	52.6°	56.3°	59.0°
	β	4.46	4.46	4.46	4.43	3.39	2.82	2.19	1.84	1.60	1.30	1.10
≤ 40	θ	36.6°	36.6°	36.6°	36.6°	41.2°	45.0°	50.2°	53.7°	56.3°	60.2°	63.0°
	β	4.06	4.06	4.06	4.06	3.20	2.62	2.00	1.66	1.43	1.14	0.95
≤ 60	θ	40.8°	40.8°	40.8°	40.8°	44.5°	49.2°	55.1°	58.9°	61.8°	65.8°	68.6°
	β	3.50	3.50	3.50	3.50	2.92	2.32	1.72	1.40	1.18	0.92	0.75
≤ 80	θ	44.3°	44.3°	44.3°	44.3°	47.1°	52.3°	58.7°	62.8°	65.7°	69.7°	72.4°
	β	3.10	3.10	3.10	3.10	2.71	2.11	1.52	1.21	1.01	0.76	0.62

$$s_{xe} = \frac{1.38 s_x}{a_g + 0.63} \tag{3.63}$$

$$\varepsilon_x = \frac{\frac{M_u}{d_v} + 0.5 N_u + 0.5\left(V_u - V_p\right)\cot\theta - A_{ps} f_{po}}{E_s A_s + E_p A_p} \tag{3.64}$$

If either value computed for ε_x is negative, the user should use **Equation 3.65** to compute the longitudinal steel strain instead.

$$\varepsilon_x = \frac{\frac{M_u}{d_v} + 0.5 N_u + 0.5\left(V_u - V_p\right)\cot\theta - A_{ps} f_{po}}{2\left(E_c A_c + E_s A_s + E_p A_p\right)} \tag{3.65}$$

where, A_c is the area of concrete on the flexural tension side, A_p is the area of prestressing steel on the flexural tension side, A_s is the area of non-prestressed steel on the flexural tension side, f_{po} is computed by the modulus of elasticity of the prestressing tendons (E_p) times the locked difference in strain at ultimate load between the prestressing tendons and the surrounding concrete, N_u is the factored axial force, s_x is the crack spacing parameter, and a_g is the maximum aggregate size in inches.

A simplified procedure is presented in the AASHTO LRFD (2010) where the values of β and θ can be calculated using the following expressions shown in **Equations 3.66** and **3.67**. The parameter s_{xe} can be calculated using **Equation 3.63**.

$$\beta = \frac{4.8}{1+750\varepsilon_x} \cdot \frac{51}{39+s_{xe}} \tag{3.66}$$

$$\theta = 29 + 3500\varepsilon_x \tag{3.67}$$

3.5.3. Canadian Standards Association, CSA A23.3-04. The Canadian Standards Association method, also based on MCFT, gives the following **Equations 3.68** to **3.76** to calculate the shear strength of a section using their general method. Note that the equations are given in psi and in. units, with the same notation defined in previous sections.

$$V_n = V_c + V_s + V_p \tag{3.68}$$

$$V_{n,max} = 0.25f'_c b_v d_v + V_p \tag{3.69}$$

$$V_c = \beta\sqrt{f'_c} b_v d_v \tag{3.70}$$

$$\beta = \frac{0.40}{1+1500\varepsilon_x} \cdot \frac{1300}{1000+s_{ze}} \tag{3.71}$$

$$s_{ze} = \frac{35 s_z}{15+a_g} \tag{3.72}$$

The term a_g should be taken as zero if f'_c exceeds 10,150 psi. The crack spacing parameter s_z can be taken as d_v or as the maximum distance between layers of distributed longitudinal reinforcement, whichever is less. Each layer of reinforcement must have an area at least equal to $0.003 b_v s_z$. However, $s_{ze} \geq 0.85 s_z$.

$$\varepsilon_x = \frac{\frac{M_u}{d_v}+0.5N_u+V_u-V_p-A_{ps}f_{po}}{2\left(E_s A_s+E_p A_p\right)} \tag{3.73}$$

$$V_s = \frac{A_v f_y d_v \cot\theta}{s} \tag{3.74}$$

$$\theta = 29 + 7000\varepsilon_x \tag{3.75}$$

$$A_{v,min} \geq 0.06\sqrt{f'_c}\,\frac{b_v s}{f_y} \tag{3.76}$$

4. EXPERIMENTAL PROGRAM

4.1. GENERAL

The objective of this study was to investigate the shear performance of reinforced concrete (RC) beams composed of RCA. The experimental program consisted of 18 tests performed on full-scale RC beams. The principal parameters investigated were:

(1) concrete type – recycled aggregate concrete (RAC) or conventional concrete (CC), and

(2) amount of longitudinal reinforcement.

Also, as part of this study, small scale testing was performed to determine hardened concrete properties such as compressive strength, flexural strength, and splitting tensile strength.

4.2. TEST BEAMS

The reinforcement for the beams was designed in accordance with the AASHTO LRFD Bridge Design Specifications (AASHTO LRFD, 2010). Each beam measured 14 ft. in length with a cross section of 12 in. x 18 in. The cross section was selected to maintain a slender beam with a shear span-to-depth ratio larger than 3.0, thus avoiding any deep beam effects. The longitudinal reinforcement was selected to ensure a shear failure prior to a flexural failure yet still remain below the maximum amount allowed by code. Each beam had two test regions, with each region measuring approximately 4 ft. in length. All of the specimens had #3 stirrups spaced at 2 in. within the bearing area to prevent premature failure as well as #3 stirrups spaced at 7 in. within the middle region to

support the reinforcing cage and prevent any premature failure outside of the shear test regions.

Table 4.1 summarizes the test matrix used in this study. The beam designation included a combination of letters and numbers: NS stands for no stirrups within the test region. The numbers 4, 6, and 8 indicate the number of #7 longitudinal reinforcement bars within the tension area of the beam section. For example, NS-6 indicates a beam with no stirrups within the test region and 6 #7 bars within the bottom of the beam. Two beams were constructed and tested for each combination of variables shown in **Table 4.1**. The cross sections for these specimens are shown in **Figure 4.1**. **Figure 4.2** shows the load pattern and location of strain gauges on the test beams.

Table 4.1: Shear Beam Test Matrix

Section	Bottom reinforcement	Top reinforcement	ρ	Stirrups
NS-4	4#7	2#4	0.0127	-
NS-6	6#7	2#4	0.0203	-
NS-8	8#7	2#7	0.0271	-

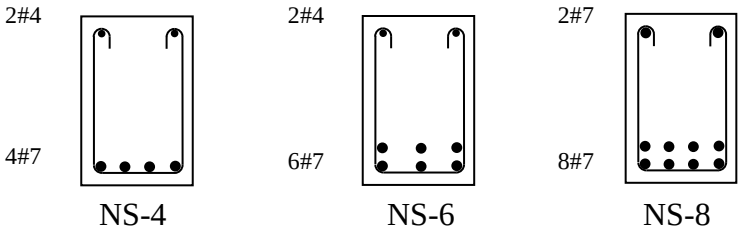

Figure 4.1: Cross Sections and Reinforcement Layout of the Beams

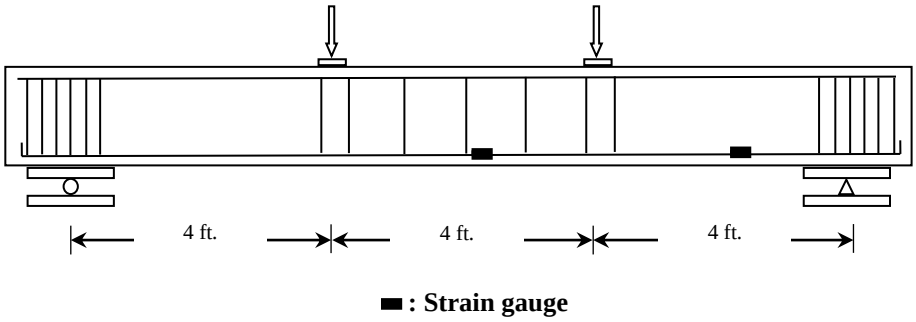

Figure 4.2: Load Pattern and Location of Strain Gauges on the Test Beams

4.3. MATERIALS

4.3.1. Concrete. For this study, three mix designs were produced and evaluated for shear performance. A MoDOT Class B air-entrained mix design was used as a baseline for reference throughout the study and also as the parent material for the recycled concrete aggregate. The specified cement content in this mix was 535 lb., the water-to-cement ratio was 0.40, the target slump was 6 in., and the design air content was 6%. The specified amount of fine aggregate as a volume of total aggregates was 40%. For this mix, the typical dosage range of the MoDOT-approved air entrainment MB-AE 90 was 0.25-4.0 fl.oz./100 lb. of cement. The typical dosage of the Type A water reducer Glenium 7500 was 5.0 – 8.0 fl.oz./100 lb. of cement.

For the CC mix, the coarse aggregate consisted of crushed limestone with a maximum nominal aggregate size of 1 in. from the Potosi Quarry (Potosi, MO) while the fine aggregate was natural sand from Missouri River Sand (Jefferson City, MO). For the RAC mixes, the coarse aggregate consisted of RCA ground from the CC mix to a nominal maximum aggregate size of 1 in., with either 50% replacement or 100% replacement of the Potosi limestone. Test results for the coarse aggregate used in the CC mix design as well as the resulting RCA are shown in **Table 4.2**. As expected, the RCA

had lower specific gravity and unit weight and considerably higher absorption. The Los Angeles abrasion test results were virtually identical.

Table 4.2: Aggregate Properties

Property	CC	RCA
Bulk Specific Gravity, Oven-Dry	2.72	2.35
Dry-Rodded Unit Weight, (lb/ft^3)	99.8	89.8
Absorption (%)	0.98	4.56
LA Abrasion (% Loss)	43	41

Tables 4.3 and **4.4** present the mix designs and representative fresh and hardened strength properties, respectively, of the CC and RAC mixes. The first mix incorporating RCA was a 50% direct replacement design. Half of the total volume of coarse aggregate in the control MoDOT Class B mix was directly substituted with the laboratory-produced RCA and is subsequently referred to as RAC-50. The second mix incorporating RCA was a 100% direct replacement design. The total volume of coarse aggregate in the control MoDOT Class B mix was directly substituted with the laboratory-produced RCA and is subsequently referred to as RAC-100. In order to maintain consistency with the control specimens, the MoDOT Class B mix specifications were used to design the RAC mixes. However, during laboratory trial batching, it was noticed from the slump test that the RAC-100 mix lacked cohesion. To remedy this situation, the mix was modified by increasing the amount of fine aggregate volume by 5% of total aggregates, which noticeably improved the cohesion of the mix.

Table 4.3: Mix Designs per Cubic Yard

	CC	RAC-50	RAC-100
Cement (Type I) (lb)	535	535	535
w/cm	0.40	0.40	0.40
Natural Coarse Aggregate (lb)	1958	979	-
Recycled Coarse Aggregate (lb)	-	846	1650
Fine Aggregate (lb)	1253	1253	1442
HRWR (fl. oz)	55	50	42
AE (fl. oz)	20	14	7

Table 4.4: Typical Fresh and Hardened Concrete Properties for CC and RCA Mixes

Property	CC	RAC-50	RAC-100
Slump (in.)	5.5	6.5	8
Air content (%)	8.5	8	6.5
Unit weight (lb/ft^3)	145.4	139.8	136.0
Split cylinder strength (psi)	505	417	370
Flexural strength (psi)	500	425	410
Fracture Energy (lb/in.)	0.82	0.71	0.57
Compressive strength (psi)	5400	4150	4350

4.3.2. Steel Reinforcement. Shear reinforcement for the test specimens consisted of A615, Grade 60 #3 reinforcing bars. Longitudinal reinforcement for the test specimens consisted of A615, Grade 60 #4 and #7 reinforcing bars. All the steel reinforcement was tested in accordance with ASTM A370 (2011) "Standard Test Methods and Definitions for Mechanical Testing of Steel Products" to obtain the mechanical properties, which are summarized in **Table 4.5**. These results are the average of three replicate specimens.

Table 4.5: Mechanical Properties of Steel Reinforcement

Bar size	**Yield strength (psi)**
#3	71,650
#4	73,970
#7	65,120

4.4. BEAM FABRICATION

All the test beams were fabricated in either the Structural Engineering High-Bay Research Laboratory (SERL) at Missouri S&T or the Donald G. Fears Structural Engineering Laboratory at the University of Oklahoma. Steel formwork was used to cast the beams. The steel cage was assembled from reinforcement that was bent in the laboratory to the desired geometry. Due to the dimension of the beams, it was possible to cast three beams at a time. After casting, the top surface of the beams was covered with burlap and plastic sheeting, and a wet surface was maintained for three days to retain moisture for proper curing. Cylinders were cured in the same environment as the test beams by placing them next to the beams. The sheeting and burlap were then removed, and the beams were allowed to air cure in the lab environment. Photographs showing the reinforcing cages and the construction process are shown in **Figures 4.3** and **4.4**, respectively.

Figure 4.3: Reinforcing Cage Assembly

(a) Formwork

(b) Concrete placement

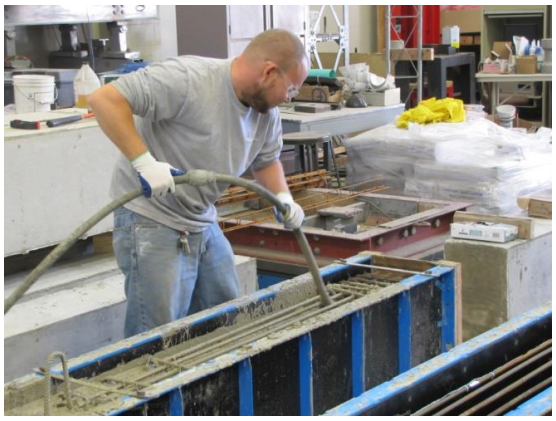

(c) Concrete consolidation

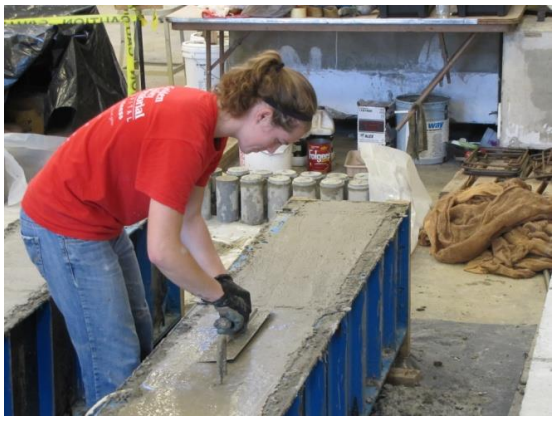

(d) Concrete finishing

Figure 4.4: Beam Construction Process

4.5. TEST SET-UP

All the specimens were tested as simply supported and subjected to third-point loading. The maximum compression capacity of the actuators available in SERL, when working individually, were insufficient to cause specimen failure. Therefore, the test set-up required the simultaneous action of two actuators as shown in **Figure 4.5**.

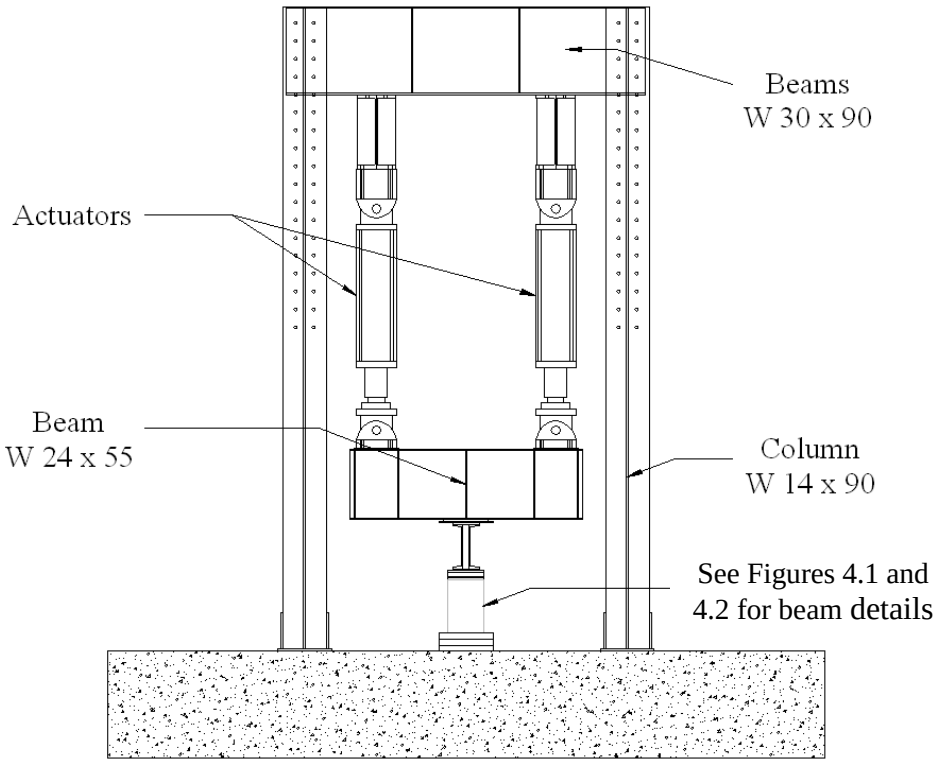

Figure 4.5: Details of Test Set-Up (1)

Two actuators, each with a 140-kip compressive capacity, were used to apply load to the beam specimens, as shown in **Figure 4.6**. The actuators applied load by pushing the steel beam downward to distribute the load onto two points of the test specimen. The loading frame assembly was designed to withstand at least two times the anticipated maximum load applied to fail the beams. Each test was performed under displacement control, and the load was applied in a series of loading steps of 0.05 in., which corresponded to a load of approximately 8 kips, until failure. Electronic measurements of strain and deformation were recorded throughout the entire loading history of the specimens, while hand measurements of strain and crack pattern formations were taken at the end of each load step while the load was paused. Each beam consisted of two test regions. The total beam length was 14 ft, with a simply supported span length of 12 ft.

The load was applied at 4 ft from each support, representing a shear span-to-depth ratio between 3.00 and 3.30 depending on the specimen, as measured from center of support to center of load. **Figure 4.7** shows a photograph of the test set-up.

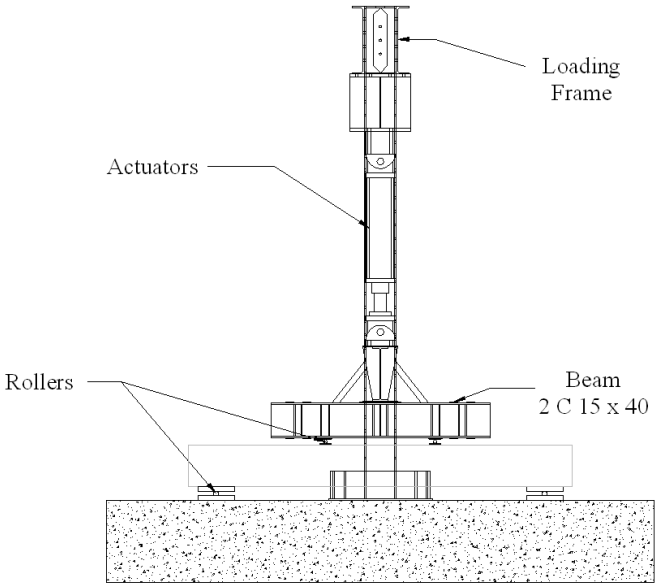

Figure 4.6: Details of Test Set-Up (2)

Figure 4.7: Photograph of Test Set-Up

4.6. INSTRUMENTATION

The specimens were instrumented with several measurement devices in order to monitor global and local deformations and strains. The load was directly measured from the load cell of the actuators. All devices were connected to a data acquisition system capable of reading up to 120 channels and all the data was recorded as shown in **Figure 4.8.**

Figure 4.8: Data Acquisition System

4.6.1. Local Deformations and Strains. Electrical resistance gauges were used to monitor local strains in the longitudinal steel reinforcement of the test region. The strain gauges were purchased from Vishay Precision Group. They were made of constantan foil with 120 ohm resistance and had a linear pattern (uniaxial) with a gauge

length of ¼ in. Two strain gauges were installed on longitudinal steel reinforcement in the test region as shown in **Figure 4.2.** The strain values obtained from the strain gauges are localized measurements at the point where the gauge is installed. The first one was located at the midpoint of the shear test region, while the second was located at mid-span.

4.6.2. Global Deformations. One Linear Variable Displacement Transducer (LVDT) was used to monitor vertical deflection of the test specimen. The LVDT was located at the midpoint of the test specimen, 3 in. below the top of the beam as shown in **Figures 4.9** and **4.10**.

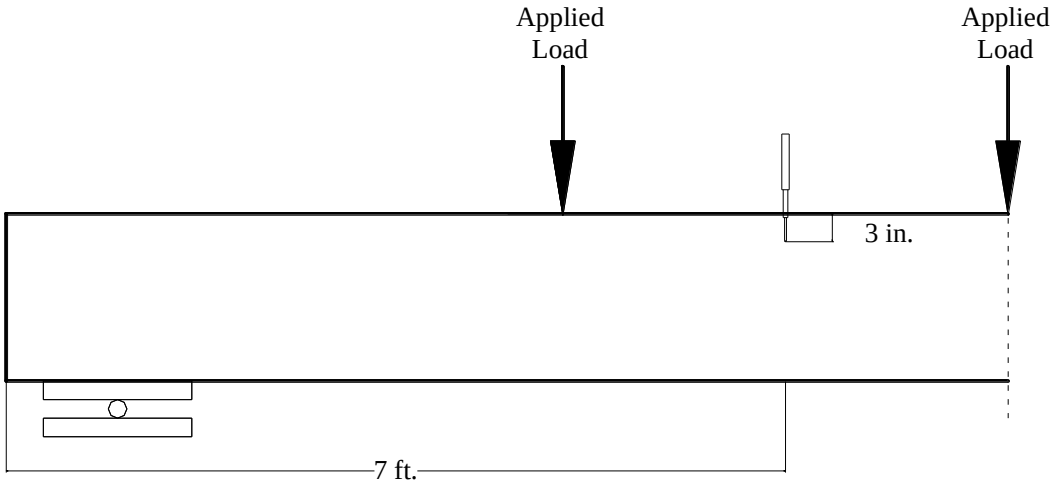

Figure 4.9: Location of LVDT to Measure Deflection

Figure 4.10: Detail of LVDT for Deflection Measurement

5. TEST RESULTS, BEHAVIOR & ANALYSIS

5.1. GENERAL

The purpose of this study was to evaluate the shear behavior of full-scale reinforced concrete (RC) beams constructed from RCA, which has not been fully investigated in previous research studies. The objectives of this section are to: (1) discuss the overall behavior of the specimens, (2) discuss the crack morphology and progression, (3) discuss the load-deflection response, (4) evaluate the failure mechanism including reinforcement strains, (5) compare the test results with predicted capacities based on applicable design standards, (6) compare the RAC test results with the control specimen results, and (7) compare the test results with a shear test database of conventional concrete specimens.

5.2. TEST RESULTS & BEHAVIOR OF FULL-SCALE SPECIMENS

Table 5.1 summarizes the compressive strength at time of testing, shear force at failure, V_{test}, average shear stress at failure, $V_{test}/b_w d$, and ratio of the average shear stress to square root of the compressive strength, $v_{test}/\sqrt{f'c}$. A useful comparison is to compare the last column in **Table 5.1** with ACI 318 (2011) Equation 11-3, rewritten in terms of average shear stress for normal weight concrete and shown as **Equation 5.1**. As shown in **Table 5.1,** comparison between the experimental shear strength and ACI 318 (2011) shear provisions shows this equation overestimates the shear strength of two beams (one for the RAC-50 mix and one for the RAC-100 mix) with low longitudinal reinforcement ratios, which has also been reported by other researchers (Collins and Kuchma 1999).

$$v_c = 2\sqrt{f_c'} \quad (5.1)$$

In addition to studying the behavior of the specimens, the crack patterns experienced by the beams were also evaluated. During testing, cracks within the test region were marked using a permanent marker after each load step. Typical crack pattern progressions are shown in **Figure 5.1**. Furthermore **Figure 5.2** shows the crack pattern for the CC and RAC-100 beams with different percentages of longitudinal reinforcement. Cracks typically began on the tension face of the beam near the loading points. As the loading progressed, the flexural cracks in the shear test region formed inclined flexure-shear cracks. The formation of the inclined flexure-shear crack did not result in immediate failure, and additional load was required prior to failure. In general, the failure crack typically extended from the beam support to the loading point on the top side of the beam.

Figure 5.3 shows the load-deflection behavior for the beams with different longitudinal reinforcement ratios (the deflection was measured at midspan). Before the first flexural cracks occurred (point A), all of the beams displayed a steep linear elastic behavior. After additional application of load, the beams eventually developed the critical flexure-shear crack, which resulted in a drop in load. As expected, sections with a higher percentage of longitudinal reinforcement generally had a higher shear capacity, which can be attributed to a combination of additional dowel action (Taylor 1972, 1974), tighter shear cracks and thus an increase in aggregate interlock, and a larger concrete compression zone due to a downward shift of the neutral axis.

Table 5.1: Test Results Summary

Mix Design	Section		f'_c psi	V^*_{test} kips	$v_{test}=V_{test}/b_w d$ psi	$v_{test}/\sqrt{f'_c}$
CC	NS-4	1	5400	27.2	144.4	2.0
		2	4960	29.2	155.0	2.2
	NS-6	1	5400	32.2	181.9	2.5
		2	4960	37.5	211.9	3.0
	NS-8	1	5400	39.0	220.3	3.0
		2	4960	38.4	216.9	3.1
RAC-50	NS-4	1	4650	26.4	140.1	2.1
		2	5170	25.1	133.2	1.9
	NS-6	1	4650	34.0	192.1	2.8
		2	5170	33.4	188.7	2.6
	NS-8	1	4650	38.6	218.1	3.2
		2	5170	37.9	214.1	3.0
RAC-100	NS-4	1	4350	25.8	136.9	2.1
		2	4950	25.4	134.8	1.9
	NS-6	1	4350	32.2	181.9	2.8
		2	4950	27.9	157.6	2.2
	NS-8	1	4350	29.5	166.7	2.5
		2	4950	31.5	178.0	2.5

*: Includes part of the load frame not registered by the load cells and also the beam self weight at a distance d from the interior face of the support plate.

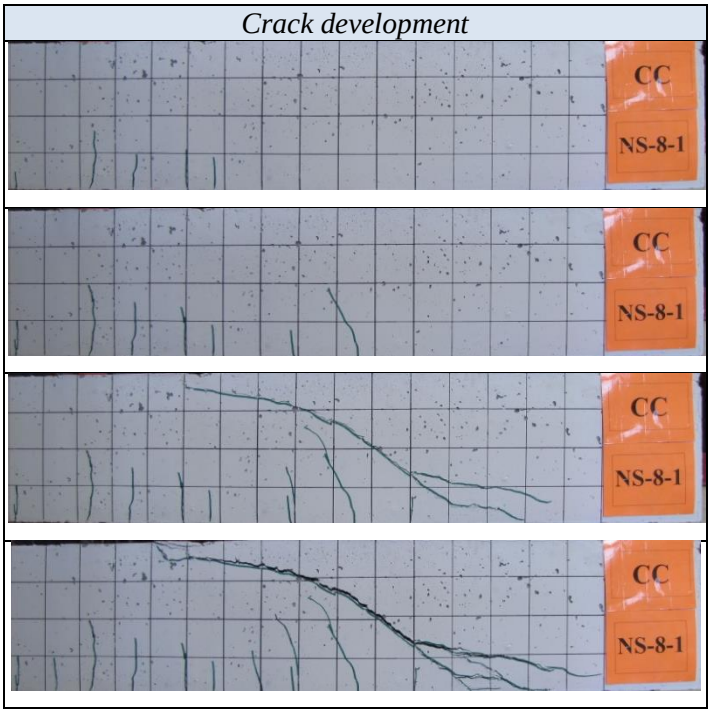

Figure 5.1: Crack Progression for the Beams

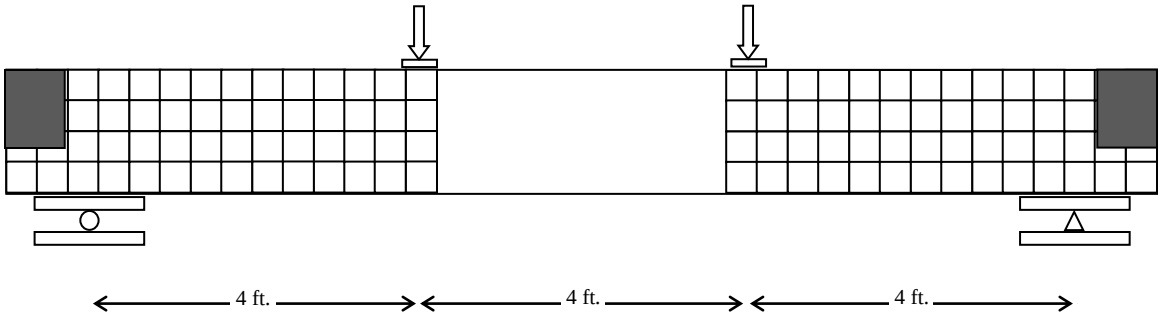

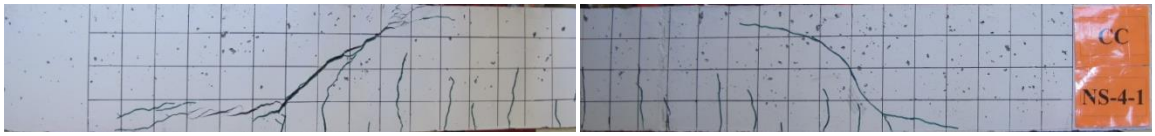

CC-NS-4-1

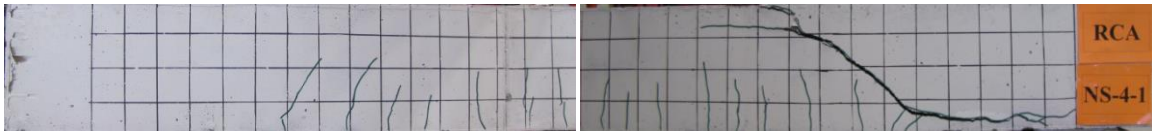

RAC-100-NS-4-1

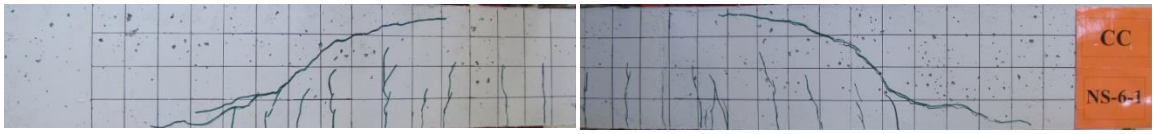

CC-NS-6-1

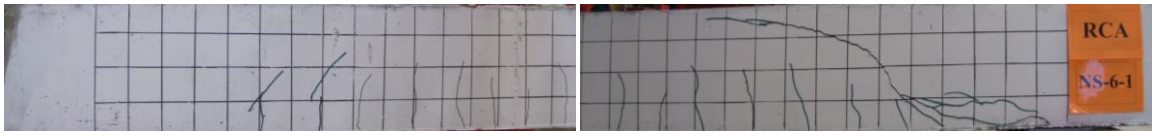

RAC-100-NS-6-1

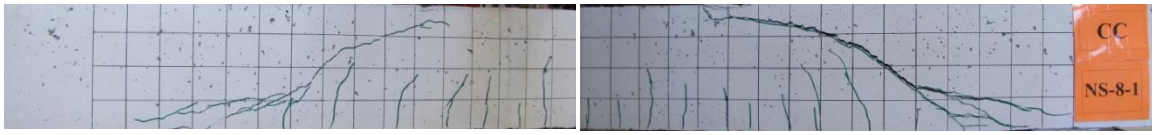

CC-NS-8-1

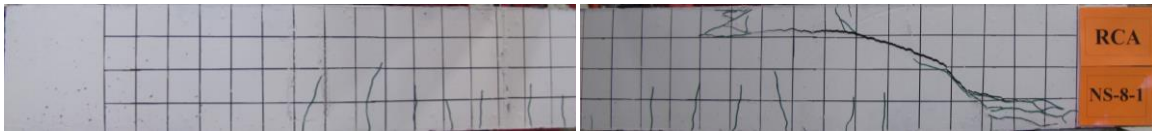

RAC-100-NS-8-1

Figure 5.2: Crack Pattern of the Beams at Shear Failure

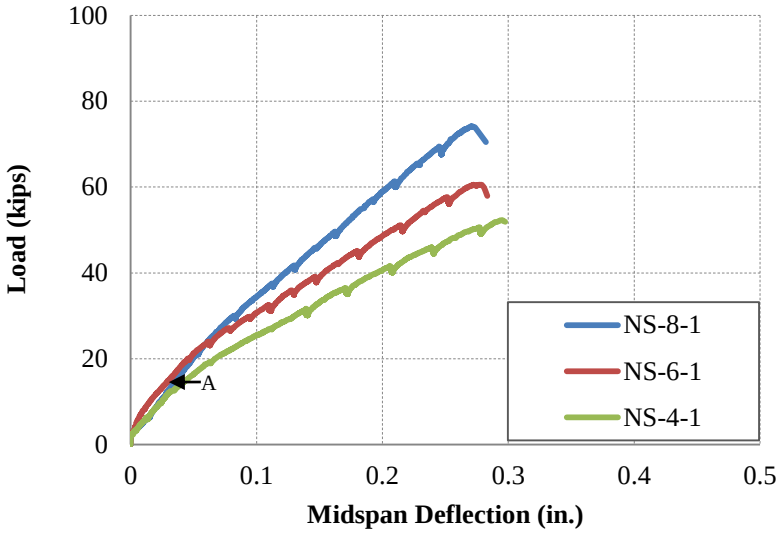

a) CC Beams

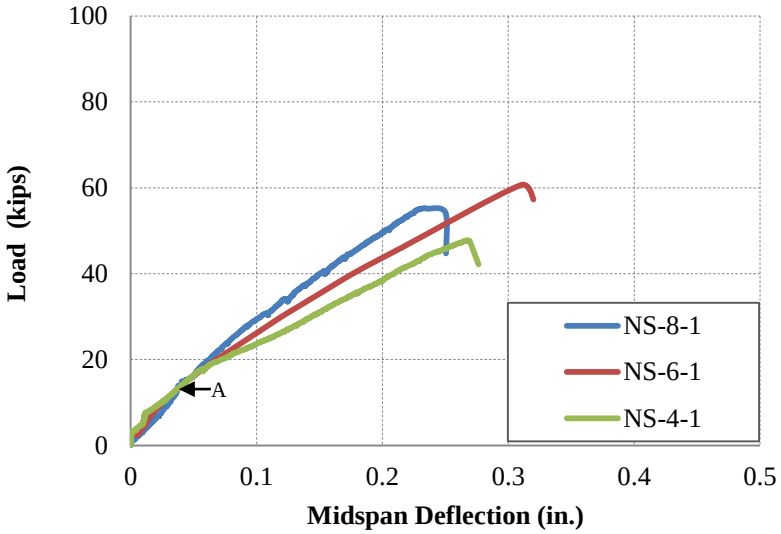

b) RAC-100 Beams

Figure 5.3: Load-Deflection Response of the Beams

5.3. COMPARISON OF REINFORCEMENT STRAINS FROM EXPERIMENT AND AASHTO LRFD (2010)

According to the AASHTO LRFD standard (2010), strain in the longitudinal tension reinforcement can be determined by

$$\varepsilon_s = \frac{\left(\frac{|M_u|}{d_v} + |V_u|\right)}{E_s A_s} \tag{5.2}$$

Table 5.2 presents the tensile strain in the longitudinal tension reinforcement at the quarter-point of the span (middle of the shear test region) obtained from both the experiments (strain gauges) and the AASHTO LRFD (2010) equation. The AASHTO LRFD equation showed good agreement with experimental results for both the CC and RAC beams.

5.4. STATISTICAL DATA ANALYSIS

Statistical tests were used to evaluate whether there is any statistically significant difference between the normalized shear strength of the CC and the RAC beams. Both parametric and nonparametric statistical tests were performed.

5.4.1. Parametric Test. The paired t-test is a statistical technique used to compare two population means. This test assumes that the differences between pairs are normally distributed. If this assumption is violated, the paired t-test may not be the most powerful test. The hypothesis for the paired t-test is as follows:

H_{o1}: The means of the normalized shear capacity of the CC is equal to the RAC-50 beams.

Table 5.2: Comparison of Reinforcement Strain from Experiment and AASHTO LRFD (2010) Equation

Section			ε_s quarter-point **Experiment**	ε_s quarter-point **Equation**	$\frac{\varepsilon_{s-Ex.}}{\varepsilon_{s-Eq.}}$
CC	NS-4	1	1039	1236	0.84
		2	1063	1136	0.94
	NS-6	1	1065	1032	1.03
		2	1105	1064	1.04
	NS-8	1	860	872	0.99
		2	858	783	1.10
	Ave.				0.99
RAC-50	NS-4	1	1001	1154	0.87
		2	912	973	0.94
	NS-6	1	1080	1064	1.01
		2	1095	1087	1.00
	NS-8	1	897	821	1.09
		2	834	768	1.09
	Ave.				1.00
RAC-100	NS-4	1	950	1000	0.95
		2	1123	984	1.14
	NS-6	1	837	872	0.96
		2	790	752	1.05
	NS-8	1	586	598	0.98
		2	414	640	0.65
	Ave.				0.95

H_{o2}: The means of the normalized shear capacity of the CC is higher than the RAC-100 beams.

$H_{a1,2}$: The means of the normalized shear capacity of the CC is not higher than the RAC-100 beams.

The statistical computer program Minitab 15 was employed to perform these statistical tests. Both Kolmogorov-Smirnov and Anderson-Darling tests showed the data, the differences between the shear capacities of the CC and the RAC beams, follows a normal distribution. Therefore, the paired t-tests could be performed. The result of the paired t-test showed that the p-values were 0.778 and 0.924 (>0.05) for the first and second hypothesis, respectively. This confirms the null hypothesis at the 0.05 significance level. In other words, the means of the normalized shear capacity of the CC was equal to the RAC-50 beams; however, it was statistically higher than the RAC-100 beams.

5.4.2. Nonparametric Test. Unlike the parametric tests, nonparametric tests are referred to as distribution-free tests. These tests have the advantage of requiring no assumption of normality, and they usually compare medians rather than means. The Wilcoxon signed-rank test is usually identified as a nonparametric alternative to the paired t-test. The hypothesis for this test is the same as those for the paired t-test. The Wilcoxon signed-rank test assumes that the distribution of the difference of pairs is symmetrical. This assumption can be checked; if the distribution is normal, it is also symmetrical. As mentioned earlier, the data follows normal distribution and the Wilcoxon signed-rank test can be used. The p-values for the Wilcoxon signed rank were 0.675 and 0.957 (>0.05) for the first and second hypothesis, respectively. That confirmed

the null hypothesis at the 0.05 significance level. Interestingly, the p-values for both the paired t-tests (parametric test) and the Wilcoxon signed rank test (nonparametric test) are very close to each other.

Overall, results of the statistical data analyses showed that the CC beams had almost the same normalized shear strength as the RAC-50 beams and higher normalized shear capacity then the RAC-100 beams.

5.5. COMPARISON OF TEST RESULTS WITH SHEAR PROVISIONS OF SELECTED STANDARDS

In the following section, the experimental shear strengths of the beams are compared with the shear provisions of the following standards: AASHTO LRFD (2010), ACI 318 (2011), and CSA (2004). For this comparison, all of the safety factors of the standards were set equal to one and all ultimate moments and shear forces were calculated without load factors.

Table 5.3 presents the ratios of experimental-to-code predicted capacity (V_{test}/V_{code}) for the selected design standards for all of the beams. In general, the ratios are lower for the AASHTO and CSA design code provisions compared with the ACI approach. As discussed in Chapter 3, the AASHTO and CSA design codes are based on a modified compression field theory while the ACI approach is entirely empirical. For the CC beams, the ratios range from 0.80 to 1.54, while the ratios range from 0.83 to 1.68 for the RAC-50 specimens and 0.76 to 1.27 for the RAC-100 beams. For both concrete types, ACI 318-11 offered the most conservative results.

Table 5.3: Comparison of Shear Strength of Experiment and Codes

Section			AASHTO	ACI	CSA
CC	NS-4	1	0.82	0.98	0.80
		2	0.95	1.10	0.93
	NS-6	1	0.94	1.24	0.92
		2	1.23	1.51	1.20
	NS-8	1	1.11	1.50	1.09
		2	1.13	1.54	1.11
	Ave.		1.03	1.31	1.01
	COV (%)		14.7	18.2	14.8
RAC-50	NS-4	1	0.91	1.10	0.89
		2	0.85	1.00	0.83
	NS-6	1	1.16	1.49	1.13
		2	1.13	1.39	1.10
	NS-8	1	1.22	1.68	1.20
		2	1.19	1.56	1.17
	Ave.		1.08	1.37	1.05
	COV (%)		14.5	19.5	14.7
RAC-100	NS-4	1	0.85	1.04	0.83
		2	0.78	0.96	0.76
	NS-6	1	1.05	1.38	1.03
		2	0.81	1.12	0.79
	NS-8	1	0.84	1.27	0.83
		2	0.86	1.27	0.85
	Ave.		0.87	1.17	0.85
	COV (%)		11.0	13.6	11.2

In looking closer at the results, the code comparisons offer some very important information. First, the design codes tend to overestimate the shear capacities of the CC, RAC-50, and RAC-100 beams at low reinforcement ratios (i.e., the ratios are less than one), which has also been reported by other researchers (Collins and Kuchma 1999). However, at higher reinforcement ratios, the ratio of experimental-to-code predicted capacity for the AASHTO and CSA provisions is greater than one for CC and RAC-50 yet less than one for the RAC-100 specimens. For AASHTO, the averages are 1.10, 1.18 and 0.89 for the CC, RAC-50, and RAC-100 specimens, and for CSA, the averages are 1.09, 1.15, and 0.88 for the CC, RAC-50, and RAC-100 test results. This result indicates that existing code provisions overestimated the shear capacity for the specimens that used 100% replacement of virgin aggregate with recycled aggregate but offer good agreement for those with aggregate replacement levels up to 50%.

5.6. COMPARISON OF TEST RESULTS WITH SHEAR TEST DATABASE

The four key parameters that affect concrete contribution to shear strength include depth of member or size effect (d), shear span to depth ratio (a/d), compressive strength of concrete (f´c), and longitudinal reinforcement ratio (ρ) (Reineck et al. 2003). To evaluate the effect of the aforementioned parameters on shear strength of the beams, the results of this study were compared with the wealth of shear test data available in the literature for CC (Reineck et al. 2003). **Figure 5.4(a-d)** presents the shear stress versus f´c, ρ, d, and a/d, respectively. Given the significant scatter of the database of previous shear test results, it is somewhat difficult to draw definitive conclusions on the current test values. Nonetheless, visually, **Figure 5.4(a-d)** seems to indicate that the CC and

RAC test results fall within the central portion of the data and follow the same general trend of the database. Furthermore, statistical analysis of the data indicates that the test results fall within a 95% confidence interval of a nonlinear regression curve fit of the database (using regression analysis to draw the best fit and 95% confidence intervals).

Figure 5.4(e) shows normalized shear strength (based on square root of compressive strength of concrete) versus longitudinal reinforcement ratio for the beams of this study and the shear database. As mentioned previously, since span-to-depth ratio plays a significant role in the shear strength of beams, **Figure 5.4(f)** shows the normalized shear strength for the beams of this study with the portion of the database that had similar span-to-depth ratios of the current study (span-to-depth ratio$\pm$ 5% [2.9-3.4]). Similar to **Figure 5.4(a - d)**, it can be seen from **Figure 5.4 (e)** and **(f)** that the test results of this current study are also within a 95% confidence interval of a nonlinear regression curve fit of the shear database and subset of the database. As a result, it would again appear that only the RAC-100 beams show slightly lower shear strength compared with the CC beams.

Although both the RAC-50 and RAC-100 test specimen results fall within the central portion of the plots and within a 95% confidence interval, the RAC-100 test results plot consistently lower, indicating decreased capacity for the specimens constructed with 100% replacement of virgin aggregate with recycled concrete.

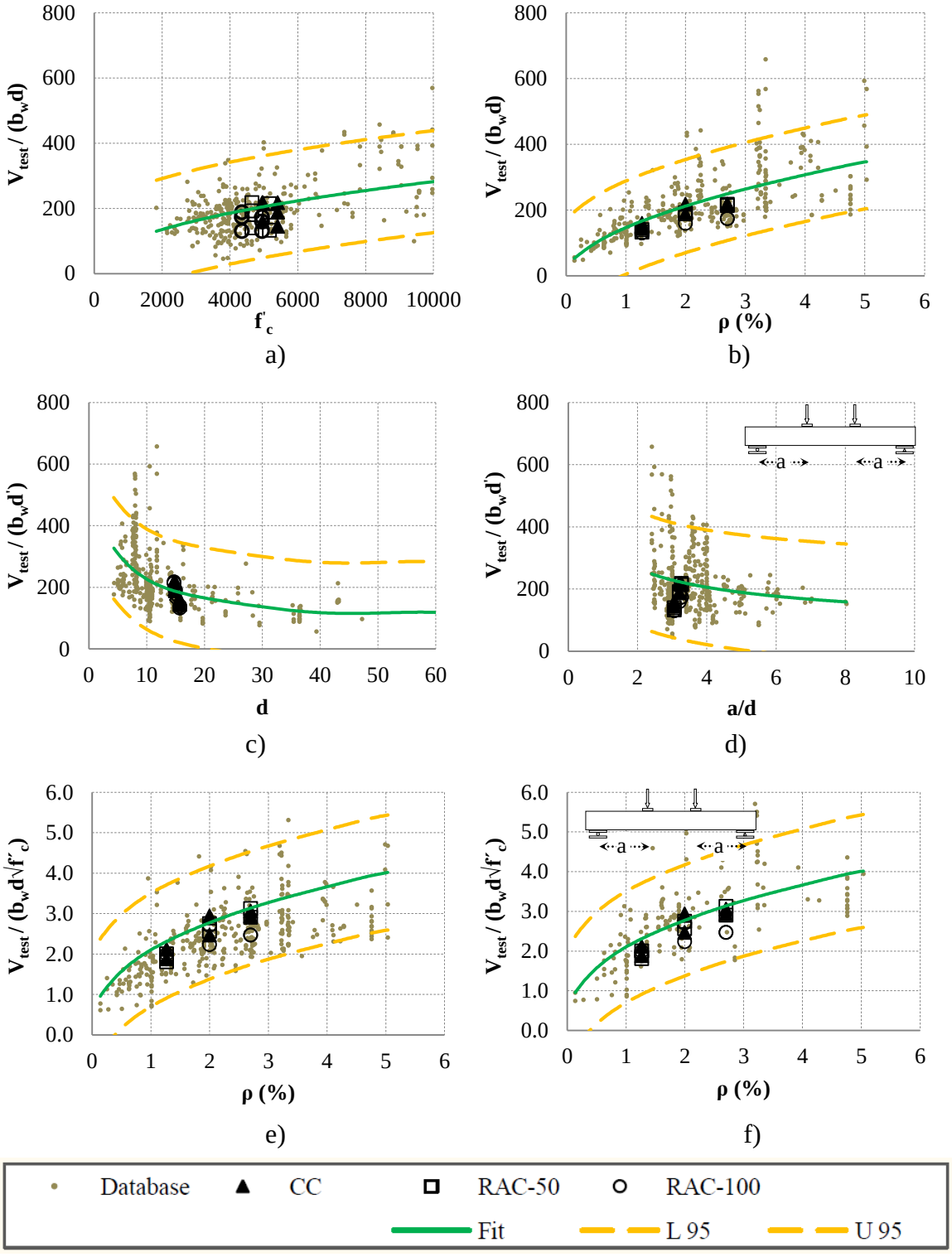

Figure 5.4: Shear Strength vs. Longitudinal Reinforcement Ratio; Results from Reineck et al. (2003) and Test Results of this Study

5.7. MATERIAL PROPERTY TEST RESULTS AND COMPARISON WITH SHEAR BEHAVIOR

Previous research and reports (ASCE-ACI Task Committee 426, 1973 and ACI Committee 445, 2009) showed that splitting tensile strength, flexural strength, and fracture energy are important parameters affecting shear strength of concrete. For this reason, the following section compares the relationship between these parameters and shear strengths for the three mixes studied in this project. To compare the shear strengths of the CC and RAC beams, the test results must be adjusted to reflect the different compressive strengths. ACI 318 (2011) provisions use the square root of the compressive strength of concrete to determine the splitting tensile strength (**Equation 5.3**), flexural strength (**Equation 5.4**), and shear strength (**Equation 5.1**) of a beam. In terms of fracture energy, Bazant's equation (**Equation 5.5**) uses a 0.46 power of the compressive strength of concrete to calculate the fracture energy of concrete. Therefore, to normalize the data for comparison, the splitting tensile strengths, flexural strengths, and shear strengths were divided by the square root of the compressive strengths of the respective concretes; however, fracture energies were divided by the compressive strengths to the power of 0.46.

$$f_{ct} = 6.7\sqrt{f_c'} \tag{5.3}$$

$$f_{ct} = 7.5\sqrt{f_c'} \tag{5.4}$$

$$G_F = 2.5\,\alpha_o \left(\frac{fc'}{0.051}\right)^{0.46} \left(1+\frac{d_a}{11.27}\right)^{0.22} \left(\frac{w}{c}\right)^{-0.30} \tag{5.5}$$

Figure 5.5 offers a comparison of the splitting tensile strength, flexural strength, fracture energy, and shear strength for the three different concretes tested in this study.

For the RAC-50 test beams, the splitting tensile strength, flexural strength, and fracture energy decreased between 1% and 6% compared to the CC, with the shear strength of the RAC-50 specimens experiencing a decrease of only 1%. However, for the RAC-100 test beams, the splitting tensile strength, flexural strength, and fracture energy decreased between 9% and 22% compared to the CC, with a corresponding reduction in shear strength of 11%. In other words, the RAC-50 mix exhibited a slight decrease in basic mechanical properties and a corresponding slight decrease in shear capacity, while the RAC-100 mix exhibited a larger decrease in basic mechanical properties and a corresponding larger decrease in shear strength.

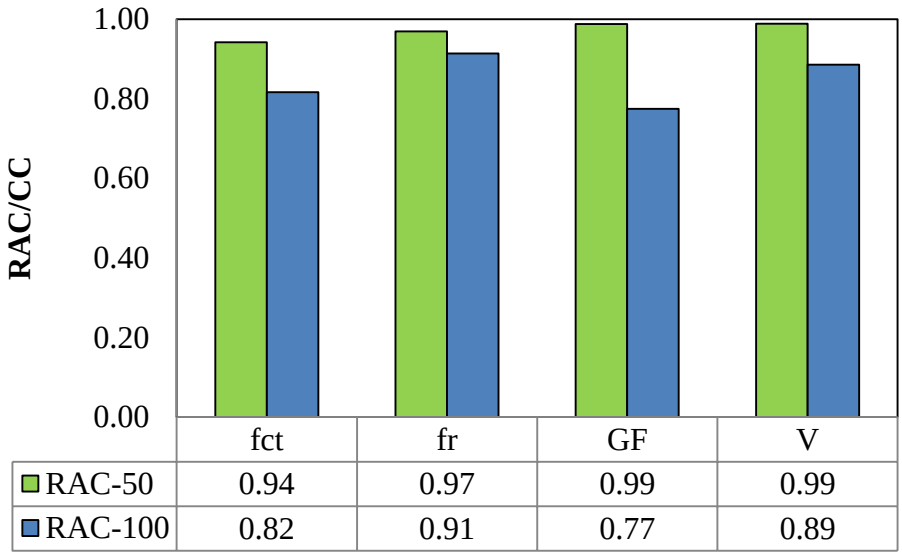

	fct	fr	GF	V
RAC-50	0.94	0.97	0.99	0.99
RAC-100	0.82	0.91	0.77	0.89

Figure 5.5: Comparison of Mechanical Properties and Shear Strengths of the CC and RAC Beams

6. FINDINGS, CONCLUSIONS, AND RECOMMENDATIONS

The main objective of this research study was to evaluate the shear behavior and response of RAC through material, component, and full-scale testing. The main feature of the experimental program consisted of 18 tests performed on full-scale reinforced concrete beams. The principal parameters investigated were: (1) concrete type – RAC vs. CC, and (2) amount of longitudinal (flexural) reinforcement. The behavior of the RAC was examined in terms of crack morphology and progression, load-deflection response, failure mechanism including critical crack angle and reinforcement strains, comparison with predicted strengths from design standards, comparison with identical CC test specimens (including statistical analyses), comparison with a shear test database of CC specimens, and, finally, comparison of basic mechanical properties related to shear strength. This section contains the findings of the test program as well as conclusions and recommendations.

6.1. FINDINGS AND CONCLUSIONS

Based on the results of this research study, the following findings are presented with regard to shear behavior and the use of recycled concrete as aggregate:

- In terms of crack morphology, crack progression, and load-deflection response, the behavior of the CC and RAC beams was virtually identical.
- Statistical data analyses – both parametric and nonparametric – showed that there was no statistically significant difference between the normalized shear capacities of the CC and the RAC-50 specimens.

- Statistical data analyses – both parametric and nonparametric – showed that there was a statistically significant difference between the normalized shear capacities of the CC and RAC-100 specimens, and as a result, the RAC-100 specimens had, on average, 11% lower shear capacity than the CC.
- Existing design standards (AASHTO, ACI, CSA) overestimated the shear capacities of the RAC-100 beams in most of the cases studied.
- Existing design standards (AASHTO, ACI, CSA) overestimated the shear capacities of all beams at low reinforcement ratios, except for the ACI code for specimens CC-NS-4-1 and RAC100-NS-4-2.
- The CC and RAC test results fall within a 95% confidence interval of a nonlinear regression curve fit of the CC shear test database.
- For the RAC-50 test beams, the splitting tensile strength, flexural strength, and fracture energy decreased between 1% and 6% compared to the CC, with the shear strength of the RAC-50 specimens experiencing a decrease of only 1%.
- For the RAC-100 test beams, the splitting tensile strength, flexural strength, and fracture energy decreased between 9% and 22% compared to the CC, with a corresponding reduction in shear strength of 11%.
- The AASHTO LRFD equation accurately estimated the reinforcement strain for both the CC and RAC beams.

Based on the findings of this research study, the following conclusions are drawn with regard to shear behavior and the use of recycled concrete as aggregate:

- Beams containing 50% replacement of virgin aggregate with RCA had normalized shear strengths comparable to conventional concrete.
- Beams containing 100% replacement of virgin aggregate with RCA had normalized shear strengths 11% lower, on average, than conventional concrete.
- The decrease in shear capacity is most likely due to the double interfacial transition zone that exists when using recycled concrete as an aggregate, and the effect is more pronounced as the percentage replacement increases.
- The decrease in basic mechanical properties (splitting tensile strength, fracture energy) for the RAC parallels the decrease in full-scale shear behavior and can be used as a predictor in mixes containing recycled concrete as aggregate.
- Although limited based on the number of variables tested in this study, it would appear that replacing more than 50% of the virgin aggregate with RCA will result in a noticeable decrease in shear capacity, 11% for the mixes studied in this investigation.

6.2. RECOMMENDATIONS

Due to the limited number of studies of the shear behavior of RAC, further research is needed to make comparisons and conclusions across a larger database. However, based on the findings and conclusions developed in this current study, the following preliminary recommendations are presented:

- Limit the percentage replacement of virgin aggregate with RCA to 50%, which should not result in any noticeable decrease in overall structural behavior compared to conventional concrete.
- Perform detailed material and full-scale specimen testing of any mixes containing more than 50% replacement of virgin aggregate with RCA.
- Additional testing is required to definitively determine whether RAC has decreased shear capacity compared to CC. This testing should investigate additional mix design variations, aggregate type and content, cross section aspect ratio, and type of loading. This database will then provide a basis for modifications to existing design standards.

BIBLIOGRAPHY

Abbas, A., Fathifazl, G., Isgor, O.B., Razaqpur, A.G., Fournier, B., and Foo, S. (2006). "Proposed Method for Determining the Residual Mortar Content of Recycled Concrete Aggregates." CSCE 2006 Annual Conference, Calgary, Alberta, Canada.

AASHTO LRFD, (2010). Bridge Design Specifications and Commentary (4th Ed.). American Association of State and Highway Transportation Officials. Washington, DC.

AASHTO T 318 (2002). Water Content of Freshly Mixed Concrete Using Microwave Oven Drying. American Association of State Highway and Transportation Officials, Washington D.C.

ACI Committee 211, (1991). Standard Practice for Selecting Proportions for Normal, Heavyweight, and Mass Concrete (ACI 211.1-91). American Concrete Institute, Farmington Hills, MI.

ACI Committee 318, (2011). Building Code Requirements for Structural Concrete and Commentary (ACI 318-08). American Concrete Institute, Farmington Hills, MI.

ACI Committee 445, (2009). Recent Approaches to Shear Design of Structural Concrete (ACI 445R-99). American Concrete Institute, Farmington Hills, MI.

ACI Committee 446, (1999). Fracture Mechanics of Concrete: Concepts, Models and Determination of Material Properties (ACI 446.1R). American Concrete Institute, Farmington Hills, MI.

ASCE-ACI Task Committee 426, (1973). The Shear Strength of Reinforced Concrete Members. ASCE Journal of the Structural Division, Vol. 99, No. 6, pp. 1091-1187.

ASCE-ACI Task Committee 445, (1998). Recent Approaches to Shear Design of Structural Concrete. ASCE Journal of Structural Engineering, Vol. 124, No. 12, pp. 1375-1417.

ASTM A370, (2011). "Standard Test Methods and Definitions for Mechanical Testing of Steel Products." American Society for Testing Materials (ASTM International).

ASTM A615/A615M, (2009). "Standard Specification for Deformed and Plain Carbon-Steel Bars for Concrete Reinforcement." ASTM, West Conshohocken, PA, 6 pp.

ASTM C127, (2007). "Standard Test Method for Density, Relative Density (Specific Gravity), and Absorption of Coarse Aggregate." American Society for Testing Materials (ASTM International).

ASTM C128, (2007). "Standard Test Method for Density, Relative Density (Specific Gravity), and Absorption of Fine Aggregate." American Society for Testing Materials (ASTM International).

ASTM C138, (2010). "Standard Test Method for Density (Unit Weight), Yield, and Air Content (Gravimetric) of Concrete." American Society for Testing Materials (ASTM International).

ASTM C192, (2007). "Standard Practice for Making and Curing Concrete Test Specimens in the Laboratory." American Society for Testing Materials (ASTM International).

ASTM C231, (2010). "Standard Test Method for Air Content of Freshly Mixed Concrete by the Pressure Method." American Society for Testing Materials (ASTM International).

ASTM C39/C39M, (2011). "Standard Test Method for Compressive Strength of Cylindrical Concrete Specimens." American Society for Testing Materials (ASTM International).

ASTM C469, (2002). "Standard Test Method for Static Modulus of Elasticity and Poisson's Ratio of Concrete in Compression." American Society for Testing Materials (ASTM International).

ASTM C496, (2004). "Standard Test Method for Splitting Tensile Strength of Cylindrical Concrete Specimens." American Society for Testing Materials (ASTM International).

ASTM C566, (1997). "Standard Test Method for Total Evaporable Moisture Content of Aggregate by Drying." American Society for Testing Materials (ASTM International).

ASTM C617, (2009). "Standard Practice for Capping Cylindrical Concrete Specimens." American Society for Testing Materials (ASTM International).

ASTM C78, (2009). "Standard Test Method for Flexural Strength of Concrete (Using Simple Beam with Third-Point Loading)." American Society for Testing Materials (ASTM International).

ASTM E178, (2008). "Standard Practice for Dealing with Outlying Observations." American Society for Testing Materials (ASTM International).

Bazant, Z.P., and Becq-Giraudon, E., (2002). "Statistical Prediction of Fracture Parameters of Concrete and Implications for Choice of Testing Standards." Cement and Concrete Research Journal, Vol. 32, No. 4, pp. 529-556.

Bazant, Z.P., and Kim, J.K., (1984). "Size Effect in Shear Failure of Longitudinally Reinforced Beams." ACI Journal Proceedings, Vol. 81, pp. 456-468.

Bazant, Z.P., and Pfeiffer, P.A., (1987). "Determination of Fracture Energy from Size Effect and Brittleness Number." ACI Materials Journal, Vol. 84, No. 6, pp. 463-480.

Bazant, Z.P., and Sun, H.H., (1987). "Size Effect in Diagonal Shear Failure: Influence of Aggregate Size and Stirrups." ACI Journal Proceedings, Vol. 84, pp. 259-272.

Bažant, Z. P., and Yu, Q., (2005). "Design against Size Effect on Shear Strength of Reinforced Concrete Beams without Stirrups," Journal of Structural Engineering, ASCE, V. 131, No. 12, pp. 1877-1885.

Bentz, E.C., Vecchio, F.J, and Collins, M.P., (2006). "Simplified Modified Compression Field Theory for Calculating Shear Strength of Reinforced Concrete Elements." ACI Structural Journal, Vol. 103, No. 4, pp. 614-624.

Boresi, A.P., and Schmidt, R.J., (2003). Advanced Mechanics of Materials (6th Ed.). John Wiley & Sons.

Choi, H. B., Yi, C. K., Cho, H. H., & Kang, K. I. (2010). "Experimental Study on the Shear Strength of Recycled Aggregate Concrete Beams." Magazine of Concrete Research, V.62 (2), pp.103-114.

Cladera, A., (2002). Shear Design of Reinforced High-Strength Concrete Beams. PhD Thesis. Universitat Politécnica de Catalunya. Barcelona, Spain.

Collins, MP, Kuchma D. (1999). "How Safe are Our Large, Lightly Reinforced Concrete Beams, Slabs, and Footings?" ACI Structural Journal, V.96, No. 4, pp. 482–90

Collins, M.P., and Mitchell, D., (1991). Prestressed Concrete Structures. Response Publications.

Collins, M.P., Bentz, E.C., and Sherwood, E.G., (2008). "Where is Shear Reinforcement Required? Review of Research Results and Design Procedures." ACI Structural Journal, Vol. 105, No. 5, pp. 590-600.

Collins, M.P., Mitchell, D., and Bentz, E.C., (2008). "Shear Design of Concrete Structures." The Structural Engineer, Vol. 86, No. 10, pp. 32-39.

Comite Euro-International du Beton, (1990). CEB-FIP Model Code 1990, Redwood Books, Wiltshire, England.

Coronado, C., (2006). Characterization, Modeling and Size Effect of Concrete-Epoxy Interfaces. PhD Thesis. Pennsylvania State University. United States of America.

CSA Committee A23.3, (2004). Design of Concrete Structures (CSA A23.3-04). Canadian Standards Association. Rexdale, ON, Canada.

Dahl, H., and Brincker, R., (1989). "Fracture Energy of High-Strength Concrete in Compression." International Conference on Fracture of Concrete and Rock: Cardiff. Elsevier Science, pp. 523-536.

Duthinh, D., (1999). "Sensitivity of Shear Strength of Reinforced Concrete and Prestressed Concrete Beams to Shear Friction and Concrete Softening According to Modified Compression Field Theory." ACI Structural Journal, Vol. 96, No. 4, pp. 495-508.

Einsfeld, R.A., and Velasco, M.S.L., (2006). "Measurement of the Ratio G_F/G_f for Numerical Analysis of Concrete Structures." Latin American Journal of Solids and Structures, Vol. 3, pp. 361-376.

Eurocode 2, (2004). Design of Concrete Structures – Part 1.1: General Rules and Rules for Buildings. EN 1992-1-1. Brussels. Belgium.

Fathifazl, G., Razaqpur, A. G., Isgor, O. B., Abbas, A., Fournier, B., & Foo, S. (2009). "Flexural performance of steel-reinforced recycled concrete beams." ACI Structural Journal, V. 106, No. 6, pp. 858-867.

FHWA State of the Practice National Review (2004). "Transportation Applications of Recycled Concrete Aggregate".

Gastebled, O.J., and May, I.M., (2001). "Fracture Mechanics Model Applied to Shear Failure of Reinforced Concrete Beams without Stirrups." ACI Structural Journal, Vol. 98, No. 2, pp. 184-190.

Ghaemmaghami, A., and Ghaemian, M., (2004). "Specific Fracture Energy Approximation of Dam Concrete." 13th World Conference on Earthquake Engineering. Paper No. 69. Vancouver, BC. Canada.

Griffith, A.A., (1920). The Phenomena of Rupture and Flow in Solids. Philosophical Transactions, Series A, Vol. 221, pp. 163-198.

Guinea, G.V., Planas, J., and Elices, M., (1992). "Measurement of the Fracture Energy Using Three-Point Bend Tests: Part 1 – Influence of Experimental Procedures." Materials and Structures. Materials and Structures, Vol. 25, pp. 212-218.

Gonzalez-Fonteboa, B., & Martinez-Abella, F. (2007). "Shear Strength of Recycled Concrete Beams." Construction and Building materials, 21(4), 887-893.

González-Fonteboa, B., Martínez-Abella, F., Martínez-Lage, I., & Eiras-López, J. (2009). "Structural Shear Behaviour of Recycled Concrete with Silica Fume." Construction and Building Materials, 23(11), 3406-3410.

Gustafsson, P.J., and Hillerborg, A., (1988). "Sensitivity in Shear Strength of Longitudinally Reinforced Concrete Beams to Fracture Energy of Concrete." ACI Journal Proceedings, Vol. 85, pp. 286-294.

Hillerborg, A., (1985). "Theoretical Basis of a Method to Determine the Fracture Energy G_F of Concrete." Materials and Structures, Vol. 18, No. 106, pp. 291-296.

Hillerborg, A., Modeer, M., and Petersson, P.E., (1976). "Analysis of Crack Formation and Crack Growth in Concrete by Means of Fracture Mechanics and Finite Elements." Cement and Concrete Research Journal, Vol. 6, pp. 773-782.

Hsu, T.T.C., (1993). Unified Theory of Reinforced Concrete. CRC Press.

Hsu, T.T.C., and Mo, Y.L., (2010). Unified Theory of Concrete Structures. John Wiley & Sons.

Irwin, G.R., Kies, J.A., and Smith, H.L., (1958). "Fracture Strength Relative to Onset and Arrest of Crack Propagation." Proceedings ASTM, Vol. 58, pp. 640-657.

Jenq, Y.S., and Shah, S.P., (1989). "Shear Resistance of Reinforced Concrete Beams – A Fracture Mechanics Approach." ACI Special Publication, Vol. 118, pp. 237-258.

Kaplan, M.F., (1961). "Crack Propagation and the Fracture of Concrete. ACI Journal Proceedings," Vol. 58, pp. 591-610.

Kellermann, W.F., (1933). "Effect of Size of Specimen, Size of Aggregate and Method of Loading upon the Uniformity of Flexural Strength Results." Public Roads, Vol. 13, No. 11, pp. 177-184.

Kesler, C.E., Naus, D.J., and Lott, J.L., (1972). "Fracture Mechanics – Its Applicability to Concrete." Proceedings of the International Conference on the Mechanical Behavior of Materials, Vol. IV, pp. 113-124, Kyoto, Japan.

Kikuchi, M., Mukai, T., & Koizumi, H. (1988). "Properties of Concrete Products Containing Recycled Aggregate." In Proc., 2nd Int. Symp. on Demolition and Reuse of Concrete and Masonry, Vol. 2, pp. 595-604.

Kim, J.K., and Park, Y.D., (1996). "Prediction of Shear Strength of Reinforced Concrete Beams without Web Reinforcement." ACI Materials Journal, Vol. 93, No. 3, pp. 213-222.

Kim, W., and White, R.N., (1991). "Initiation of Shear Cracking in Reinforced Concrete Beams with No Web Reinforcement." ACI Structural Journal, Vol. 88, No. 3, pp. 301-308.

Kuchma, D., (2009). "Contribution of Stirrups to Shear Resistance." Structures Congress 2009: Don't Mess with Structural Engineers, ASCE, pp. 1587-1594.

Laskar, A., Hsu, T.T.C., and Mo, Y.L.C., (2010). "Shear Strengths of Prestressed Concrete Beams Part 1: Experiments and Shear Design Equations." ACI Structural Journal, Vol. 107, No. 3, pp. 330-339.

Loov, R.E., (1998). "Review of A23.3-94 Simplified Method of Shear Design and Comparison with Results using Shear Friction." Canadian Journal of Civil Engineering, Vol. 25, No. 3, pp. 437-450.

Marotta, T.W., Coffey, J.C., LaFleur, C.B., and LaPlante, C., (2011). Basic Construction Materials (8th Ed.). Pearson-Prentice Hall.

Martin, J., Stanton, J., Mitra, N., and Lowes, L.N., (2007). "Experimental Testing to Determine Concrete Fracture Energy Using Simple Laboratory Test Setup." ACI Materials Journal, Vol. 104, No. 6, pp. 575-584.

Maruyama, I., Sogo, M., Sogabe, T., Sato, R., & Kawai, K. (2004). "Flexural Properties of Reinforced Recycled Concrete Beams." In Internacional RILEM conference on the Use of Recycled Materials in Buildings and Structures, Paper No.315, Barcelona, Spain.

Mindess, S., Young, J.F., and Darwin, D., (2003). Concrete (2nd Ed.). Prentice Hall.

Mörsch, E., (1902). Der Eisenbetonbau, Seine Theorie und Anwendung. Stuggart, Germany.

Neville, A.M., (1997). Properties of Concrete (4th Ed.). John Wiley & Sons.

Nielsen, K.E.C., (1954). "Effect of Various Factors on the Flexural Strength of Concrete Tests Beams." Magazine of Concrete Research, No. 15, pp. 105-114.

Nilson, A.H., Darwin, D., and Dolan, C.W., (2004). Design of Concrete Structures (13th Ed.). McGraw Hill.

Park, R., and Paulay, T., (1975). Reinforced Concrete Structures. John Wiley & Sons.

Rangan, B.V., (1991). "Web Crushing Strength of Reinforced and Prestressed Concrete Beams." ACI Structural Journal, Vol. 88, No. 1, pp. 12-16.

Reineck, KH, Kuchma, DA, Kim, KS; and Marx, S., (2003). "Shear Database for Reinforced Concrete Members without Shear Reinforcement," ACI Structural Journal, V. 100, No. 2, pp. 240-249.

Raphael, J.M., (1984). "Tensile Strength of Concrete." Concrete International, Vol. 81, No. 2, pp. 158-165.

RILEM TC 89-FMT Fracture Mechanics of Concrete-Test Methods, (1990). Determination of Fracture Parameters (K_{IC} and $CTOD_C$) of Plain Concrete Using Three-Point Bend Tests. Materials and Structures, Vol. 23, pp. 457-460.

RILEM TC 89-FMT Fracture Mechanics of Concrete-Test Methods, (1990). Size Effect Method for Determining Fracture Energy and Process Zone Size of Concrete. Materials and Structures, Vol. 23, pp. 461-465.

Ritter, W., (1899). Die Bauweise Hennebique. Schweizerische Bauzeitung. Zurich, Switzerland.

Schlaich, J., Schäfer, K., and Jennewein, M., (1987). "Towards a Consistent Design of Structural Concrete." PCI Journal, Vol. 32, No. 3, pp. 74-150.

Schubert, S., Hoffmann, C., Leemann, A., Moser, K., & Motavalli, M. (2012). "Recycled Aggregate Concrete: Experimental Shear Resistance of Slabs without Shear Reinforcement." Engineering Structures, 41, 490-497.

Shah, S.G., Bhasya, V., and Chandra Kishen, J.M., (2011). "Tension-Softening Properties for Concrete-Concrete Interfaces." ACI Structural Journal, Vol. 108, No. 6, pp. 725-734.

Shah, S.P., and Carpinteri, A., (1991). Fracture Mechanics Test Methods for Concrete: Report of Technical Committee 89-FMT (1st Ed.). Chapman and Hall.

So, K.O., and Karihaloo, B.L., (1993). "Shear Capacity of Longitudinally Reinforced Beams – A Fracture Mechanics Approach." ACI Structural Journal, Vol. 90, No. 6, pp. 591-600.

Taylor, HPJ. (1972). "Shear Strength of Large Beams," Journal of the Structural Division, ASCE, V. 98, No. ST11, Nov., pp. 2473-2489.

Taylor, HPJ. (1974). "The Fundamental Behavior of Reinforced Concrete Beams in Bending and Shear," American Concrete Institute, Shear in Reinforced Concrete, SP-42, pp. 43-77.

Tureyen, A.K., (2001). Influence of Longitudinal Reinforcement Type on the Shear Strength of Reinforced Concrete Beams without Transverse Reinforcement. PhD Thesis. Purdue University. United States of America.

Tureyen, A.K, and Frosch, R.J., (2003). "Concrete Shear Strength: Another Perspective." ACI Structural Journal, Vol. 100, No. 5, pp. 609-615.

Van der Veen, C., (1990). Cryogenic Bond Stress-Slip Relationship. MS Thesis. Delft University. Delft, Netherlands.

Vecchio, F.J., and Collins, M.P., (1986). "The Modified Compression Field Theory for Reinforced Concrete Elements Subjected to Shear." ACI Journal Proceedings, Vol. 83, No. 2, pp. 219-231.

Vecchio, F.J., and Collins, M.P., (1993). "Compression Response of Cracked Reinforced Concrete." Journal of Structural Engineering, Vol. 119, No. 12, pp. 3590-3610.

Walraven, J.C., (1980). Aggregate Interlock: a Theoretical and Experimental Analysis. PhD Thesis. Delft University of Technology. Delft, Netherlands.

Whitney, C.S., (1937). "Design of Reinforced Concrete Members under Flexure or Combined Flexure and Direct Compression." ACI Journal Proceedings, Vol. 33, No. 3, pp. 483-498.

Wight, J.K., and MacGregor, J.G., (2009). Reinforced Concrete Mechanics and Design (5^{th} Ed.). Pearson-Prentice Hall.

World Business Council for Sustainable Development (WBCSD) Report (2012). "Recycling concrete" http://www.wbcsdcement.org/index.php/key-issues/sustainability-with-concrete/54, Accessed date: August 2013.

Wright, P.J.F, (1955). "Comments on an Indirect Tensile Test on Concrete Cylinders." Magazine of Concrete Research, Vol. 7, No. 20, pp. 87-96.

Xiao, J., Xie, H., & Yang, Z. (2012). "Shear Transfer Across a Crack in Recycled Aggregate Concrete." Cement and Concrete Research, V. 42, pp. 700-709.

Zakaria, M., Ueda, T., Wu, Z., and Meng, L., (2009). "Experimental Investigation on Shear Cracking Behavior in Reinforced Concrete Beams with Shear Reinforcement." Journal of Advanced Concrete Technology, Vol. 7, No. 1, pp. 79-96.